



# Defective tubulin detyrosination causes structural brain abnormalities with cognitive deficiency in humans and mice

Alistair T. Pagnamenta, Pierre Heemeryck, Hilary Martin, Christophe Bosc, Leticia Peris, Ivy Uszynski, Sylvie Gory-Fauré, Simon Couly, Charu Deshpande, Ata Siddiqui, et al.

## ► To cite this version:

Alistair T. Pagnamenta, Pierre Heemeryck, Hilary Martin, Christophe Bosc, Leticia Peris, et al.. Defective tubulin detyrosination causes structural brain abnormalities with cognitive deficiency in humans and mice. Human Molecular Genetics, 2019, 10.1093/hmg/ddz186 . hal-02345641

**HAL Id: hal-02345641**

**<https://hal.science/hal-02345641>**

Submitted on 3 Dec 2020

**HAL** is a multi-disciplinary open access archive for the deposit and dissemination of scientific research documents, whether they are published or not. The documents may come from teaching and research institutions in France or abroad, or from public or private research centers.

L'archive ouverte pluridisciplinaire **HAL**, est destinée au dépôt et à la diffusion de documents scientifiques de niveau recherche, publiés ou non, émanant des établissements d'enseignement et de recherche français ou étrangers, des laboratoires publics ou privés.

# **Defective tubulin detyrosination causes structural brain abnormalities with cognitive deficiency in humans and mice**

Alistair T. Pagnamenta,<sup>1,13</sup> Pierre Heemeryck,<sup>2,13</sup> Hilary C. Martin,<sup>3,13</sup> Christophe Bosc,<sup>2</sup> Leticia Peris,<sup>2</sup> Ivy Uszynski,<sup>2</sup> Sylvie Gory-Fauré,<sup>2</sup> Simon Couly,<sup>4</sup> Charu Deshpande,<sup>5</sup> Ata Siddiqui,<sup>6</sup> Alaa A. Elmonairy,<sup>7</sup> WGS500 consortium,<sup>¶</sup> Genomics England Research Consortium,<sup>¶</sup> Sandeep Jayawant,<sup>8</sup> Sarada Murthy,<sup>9</sup> Ian Walker,<sup>10</sup> Lucy Loong,<sup>11</sup> Peter Bauer,<sup>12</sup> Frédérique Vossier,<sup>2</sup> Eric Denarier,<sup>2</sup> Tangui Maurice,<sup>4</sup> Emmanuel L. Barbier,<sup>2</sup> Jean-Christophe Deloulme,<sup>2</sup> Jenny C. Taylor,<sup>1,14</sup> Edward M. Blair,<sup>11,14,\*</sup> Annie Andrieux,<sup>2,14</sup> and Marie-Jo Moutin<sup>2,14,\*</sup>

<sup>1</sup>NIHR Oxford BRC, Wellcome Centre for Human Genetics, University of Oxford, Oxford, UK; <sup>2</sup>Univ. Grenoble Alpes, Inserm, U1216, CEA, CNRS, Grenoble Institut Neurosciences, 38000 Grenoble, France; <sup>3</sup>Wellcome Sanger Institute, Wellcome Genome Campus, Hinxton, UK; <sup>4</sup>MMDN, Univ. Montpellier, INSERM, EPHE, UMR\_S1198, Montpellier, France; <sup>5</sup>South East Thames Regional Genetics Unit, Guys and St Thomas NHS Trust, London, UK; <sup>6</sup>Department of Neuroradiology, Kings College Hospital, Denmark Hill, London SE5 9RS, UK; <sup>7</sup>Ministry of Health, Kuwait Medical Genetics Center, Sulaibikhat 80901, Kuwait; <sup>8</sup>Department of Paediatric Neurology, John Radcliffe Hospital, Oxford, UK; <sup>9</sup>Community Paediatrics, Upton Hospital, Slough, UK; <sup>10</sup>Clinical Biochemistry, Wexham Park Hospital, Slough, UK; <sup>11</sup>Oxford Centre for Genomic Medicine, Oxford University Hospitals NHS Foundation Trust, Oxford, UK; <sup>12</sup>Centogene AG, 18055 Rostock, Germany; <sup>13</sup>These authors contributed equally to this work; <sup>14</sup>These authors contributed equally to this work.

<sup>¶</sup>Full list of authors is included in the Supplemental Material under “Extended Authors”

\*Correspondence: [Ed.Blair@ouh.nhs.uk](mailto:Ed.Blair@ouh.nhs.uk); [moutinm@univ-grenoble-alpes.fr](mailto:moutinm@univ-grenoble-alpes.fr)

## Abstract

Reversible detyrosination of tubulin, the building block of microtubules, is crucial for neuronal physiology. Enzymes responsible for detyrosination were recently identified as complexes of vasohibins 1 or 2 with small vasohibin-binding protein (SVBP). Here we report three consanguineous families, each containing multiple individuals with biallelic inactivation of SVBP caused by truncating variants (p.Q28\* and p.K13Nfs\*18). Affected individuals show brain abnormalities with microcephaly, intellectual disability and delayed gross motor and speech development. Immunoblot testing in cells with pathogenic *SVBP* variants demonstrated that the encoded proteins were unstable and non-functional, resulting in a complete loss of vasohibin detyrosination activity. SVBP knock-out mice exhibit drastic accumulation of tyrosinated tubulin and a reduction of detyrosinated tubulin in brain tissue. Similar alterations in tubulin tyrosination levels were observed in cultured neurons and associated with defects in axonal differentiation and architecture. Morphological analysis of the SVBP knockout mouse brains by anatomical MRI showed a broad impact of SVBP loss, with a 7% brain volume decrease, numerous structural defects and a 30% reduction of some white matter tracts. SVBP knockout mice display behavioral defects, including mild hyperactivity, lower anxiety and impaired social behavior. They do not, however, show prominent memory defects. Thus, SVBP deficient mice recapitulate several features observed in human patients. Altogether, our data demonstrate that deleterious variants in *SVBP* cause this neurodevelopmental pathology, by leading to a major change in brain tubulin tyrosination and alteration of microtubule dynamics and neuron physiology.

## Introduction

Microtubules are dynamic, polarized polymers composed of  $\alpha/\beta$  tubulin dimers which have a wide range of cellular functions. They are crucial to cell division, cell shape and motility, and intracellular organization and transport. Thus, microtubules are key to normal development of the central nervous system. In recent years an increasing number of human brain malformations and neurological disorders have been associated with mutations in  $\alpha$  and  $\beta$  tubulin genes (1, 2). Examples of genes associated with these “tubulinopathies” include *TUB1A* and *TUBB2B* where mutations in these genes result in a range of cortical malformations such as lissencephaly and polymicrogyria (3-6). Moreover, deficiency of some microtubule binding proteins such as DCX, LIS1 or MAP1B are also well known to cause severe neurodevelopmental disorders (7, 8).

Microtubules display functional specialization by not only having several tubulin isoforms but also through diverse post-translational modifications occurring generally at their C-termini which are located on the microtubule surface. These modifications control interactions with the many microtubule-associated proteins including molecular motors and stabilizing/destabilizing proteins. Among them is the reversible detyrosination of  $\alpha$ -tubulin. Detyrosinated tubulin is generally thought to be associated with longer-lived microtubules, whereas more dynamic microtubules are mostly tyrosinated (9, 10). In the cycle of detyrosination/tyrosination, the C-terminal tyrosine of  $\alpha$ -tubulin is removed by a carboxypeptidase and re-added by a ligase. The enzyme catalyzing the tyrosination, the tubulin tyrosine ligase (TTL), was identified over 25 years ago (11) and mice lacking this enzyme have been shown to die perinatally, with poorly developed neuronal networks (12). In contrast, enzymes catalyzing the detyrosination (tubulin carboxypeptidases, TCPs) were discovered only very recently (13, 14). Vasohibins (VASHs) were shown to be the major tubulin detyrosinating

enzymes, and their partner SVBP (small vasohibin binding protein) to be a prominent regulator of their stability and activity (15-17). SVBP binds to vasohibins with high affinity (17, 18) and the tubulin carboxypeptidase function is achieved by the VASH-SVBP complexes.

Tyrosination is an important regulatory signal for neuronal physiology. It is involved in brain development and neuron functioning, including axonal guidance, neurite extension and retrograde transport (12, 19-24). Moreover, knock-down experiments for each of the proteins in the detyrosinating VASH-SVBP complex were recently shown to cause severe neuronal differentiation defects and to alter neuronal migration in the developing mouse brain (13). Interaction of VASH with SVBP and association of the complex to microtubules was shown to regulate axon specification of neurons (17).

Using a combination of whole-genome sequencing (WGS) and whole-exome sequencing (WES) we now show that biallelic inactivating *SVBP* variants in humans cause a syndrome involving brain anomalies, intellectual disability and delayed gross motor and speech development. We demonstrate that the *Svbp* knockout mouse model recapitulates several aspects of the neuropathology observed in the human subjects.

## Results

### Clinical descriptions of patients with *SVBP* mutations

#### Family 1

The proband (individual V-6) is the 6th child in a sibship of 7 surviving children (Figure 1a) born to first-cousin parents of South Asian ancestry. She showed early signs of gross motor developmental delay, sitting at 9 months, standing at 19 months and was over 2 years of age before she walked independently. She has gained a few single words of expressive language. She is relatively microcephalic (Table S1). She developed lower limb spasticity with brisk tendon reflexes. She received a number of botulinum toxin injections to relieve Achilles

contractures. She has marked mirror movements of her fingers. Cranial nerve examination is normal. She has very short 3rd and 4th toes on both feet. An MRI scan of the brain showed irregular ventricular margins and a thin corpus callosum.

Individual V-7 is the younger sister of the proband. She presented in a similar fashion to her sister with severe global developmental delay and an evolving spastic paraparesis. She also sat at 9 months, stood at 13 months and walked at 24 months. She has developed only a few single words of speech. She had a single episode of status epilepticus as a two-year-old and had an ongoing seizure disorder which resolved in adolescence. She also displays mirror movements of the fingers. Her head circumference was noted to be below the 0.4th centile for her age. Her height is between the 9th and 25th centiles. An MRI brain scan performed at age 4 years showed a small corpus callosum with dysmorphic ventricles. There was slight prominence of CSF spaces in keeping with a degree of volume loss, including the lateral cerebellar hemispheres. The cisterna magna was normal. There was completed myelination with no white matter abnormality and normal deep grey structures.

Individual IV-3 is the maternal aunt of the proband. Prior to her niece being referred to our service, she had been diagnosed with learning disability and short stature. She was noted to have short 3rd, 4th and 5th metacarpals which resulted in her being investigated for pseudohypoparathyroidism. However, all biochemical and metabolic investigations, including sequence analysis of *GNAS1* identified no specific underlying cause. At 43 years of age she has very little speech. She had marked wasting of the intrinsic muscles of her hands with clawing of the fingers. She has delayed gross motor development and walks with the use of a frame. No cranial MRI was available.

Individual IV-4 is the maternal uncle of the proband. He was 37 years of age when first seen in our clinic. He also has learning disability with a spastic paraparesis requiring several operations to release contractures at his hips and ankles. He had seizures as an infant and child,

resolving in adolescence. He walked at 5 years and has attained only a few single words of expressive language. He has hypothyroidism. He has coarse facial features similar to those seen in his affected sister and nieces. His thumbs are short and he has marked muscle wasting of the small muscles of his hands with clawing of his fingers. He has a spastic paraparesis with brisk lower limb reflexes and extensor plantar responses. No cranial MRI was available.

## **Family 2**

The proband (II-3) is a 6-year-old female referred to the Kuwait medical centre aged 2 years due to developmental delay. She is the third of four offspring (Figure 1b), born weighing 2.9 kg to phenotypically normal 1st-cousin-once-removed parents of Kuwaiti ancestry. Increased muscle tone was observed, especially in both lower limbs. She has ankle clonus, easily elicited reflexes and an unsteady spastic gait with toe walking. Occipital frontal circumference (OFC) was <0.4th centile. At age 6 she could speak only a few words. MRI of her brain showed a thin corpus callosum with dilated ventricles and poor white matter volume. Cranial nerves examinations, electromyography, plasma amino acids and urinary organic acids were all normal.

Her elder brother (II-2) is similarly affected with an OFC of 49.7 cm aged 7 years (0.4th centile). He has generalized hypertonia predominantly in the lower limbs, brisk reflexes, an unsteady spastic gait, mirror hand movement and spoke using only a few words.

## **Family 3**

The proband (II-3, Figure 1c) is the third child of first-cousin parents from a multiply consanguineous South Asian family. She was referred to the genetics clinic at 3 years of age with progressive microcephaly, progressive difficulty in walking and global developmental delay. The antenatal scans were reportedly normal and her birth weight was 2.7 kg at term (10th centile). Head circumference at birth was 31.5 cm (<0.4th centile). There were no concerns in early infancy and she was walking independently at 14 months of age but remained unsteady

on her feet and would trip easily. Upon examination she was seen to be of proportionate short stature and a failure to thrive had been noted. She also demonstrated spasticity with delayed gross and fine motor development. She has profound intellectual disability with delayed speech and language development and demonstrated autistic behavior. Neurometabolic investigations were normal. Hyperpigmentation of the skin in the form of small café au lait macules was noted. In view of the microcephaly and the café au lait macules, a DNA repair disorder was considered as a possible differential diagnosis.

Her older sibling (II-1) was initially assessed at 3 years of age because of microcephaly, progressive difficulty in walking and developmental delay. His birth weight and head circumference were reported on the 3rd centile although no measurements were available. At 3 years of age his head circumference was 46 cm (<0.4th centile). He was subsequently lost to follow-up and was seen with his younger sister when he was 21 years old. At that time, he had only 10 words. He had spastic diplegia and was non-ambulant. Additional features included 2-4 toe cutaneous syndactyly and coarse facial features.

## **Genetic findings**

### **Family 1**

We first identified a consanguineous family of Pakistani ancestry in which four individuals, two sisters and their uncle and aunt, had a syndrome characterized by learning disability, spastic paraparesis, a thin corpus callosum and decreased cerebral white matter volume (Table S1). Individual V-6 underwent WGS as part of the WGS500 project. We carried out linkage analysis under a recessive model, combining the WGS data with SNP array data from other relatives (Figure 1a). This revealed a single significant linkage peak (Figure S1): a 12.7 Mb region on chr1:40,921,145-53,713,336 (GRCh37/hg19) that had a LOD score of 3.01 and was

homozygous in all affected individuals. This region contained 145 protein-coding genes, and was interrogated for rare simple recessive variants in the WGS data.

There was only one coding variant that was sufficiently rare and that disrupted a well conserved position. This was a homozygous transition, chr1:43,282,134G>A which predicts a LoF variant c.82C>T; p.Q28\* in *SVBP* (NM\_199342.4). The variant co-segregated with the phenotype in all family members for whom DNA was available. It was seen in a single heterozygous individual from a population cohort of 7,446 exome-sequenced British Pakistani and Bangladeshi adults (East London Genes and Health; [www.genesandhealth.org/research/scientific-data-downloads](http://www.genesandhealth.org/research/scientific-data-downloads)), but absent from the gnomAD resource of 123,136 exomes and 15,496 genomes from individuals without severe paediatric disease (<https://gnomad.broadinstitute.org>). There were also no high-confidence homozygous LoF variants in either of these cohorts. We also searched for potentially causal variants under other inheritance models and outside the coding region in this family (see Supplemental Methods), but found none more likely to be pathogenic than the LoF variant in *SVBP*.

## Family 2

In the hope of replicating the results from Family 1, we searched the CentoMD mutation database (25) for candidate variants in *SVBP* and identified a 5 year old female (II-3, CentoGene ID 1099053) with a homozygous c.39\_42del; p.K13Nfs\*18. This variant had been identified by trio WES analysis, with the unaffected parents both shown to be heterozygous. The only other potential candidate variant identified in this family highlighted was a c.3049G>A; p.E1017K in *SZT2* (NM\_015284.3), a gene associated with Early Infantile Epileptic Encephalopathy (OMIM \*615463). Both *SVBP* and *SZT2* variants were homozygous in the elder affected brother (II-2). DNA from unaffected siblings has not yet been tested, however the proximity of *SZT2* to *SVBP* means the variants will likely co-segregate and thus testing unaffected siblings

is unlikely to rule *SZT2* out conclusively. However, *SZT2* is a large gene and c.3049G>A predicts a missense change with poor SIFT and polyphen scores. Most variants in this gene which have been reported to be pathogenic in ClinVar ([www.ncbi.nlm.nih.gov/clinvar/](http://www.ncbi.nlm.nih.gov/clinvar/)) are LoF alleles. Epilepsy is a common feature whereas II-3 had no history of seizures. The *SZT2* variant was therefore assessed as being one of unknown significance. The proband's similarly affected brother (II-2) had previously undergone exome analysis in another laboratory and this had identified variants in *PLP1* (c.-102C>T) and *WDR81* (c.2051A>C; p.Q684P). Segregation analysis of these two variants in the parents and in II-3 excluded both variants from being causative for the phenotype.

### Family 3

By searching through genetic data from 49,434 individuals from the 100,000 Genomes Project, we identified one additional family with biallelic LoF variants in *SVBP*. Both affected children in this family had been diagnosed with intellectual disability and were homozygous for the same c.82C>T; p.Q28\* variant as seen in Family 1. Both unaffected siblings were heterozygous for this variant (Figure 1c). Using SNP array data, Families 1 and 3 were shown to share a 3.9 Mb region of identity by descent on chromosome 1, between rs9659165 and rs7515271. Using WGS, this shared region was refined to 39,550,261 – 43,442,698 (rs76104968 and rs1770796). The chr1:43,282,134G>A (p.Q28\*) variant is thus likely to be an ancestral variant rather than a recurrent mutation.

### Clinical comparison across families

Clinical details for affected individuals are reported in Table S1. Most individuals exhibited microcephaly (on or below the 0.4<sup>th</sup> centile, where data were available), moderate to severe learning disability and speech delay. A detailed comparison of the MRI data available in these

families demonstrated a subtle but consistent pattern comprising reduced brain volume, a thin corpus callosum and abnormal ventricles in all three families (Figure 1 d,e and data not shown). Affected individuals also exhibited spasticity and in most cases this involved predominantly the lower limbs. More variable features included mirror movements observed in 4/8, coarse facial features in 5/8, seizures in 3/8, short stature in 3/8 and digital abnormalities in 4/8.

### **Consequences of *SVBP* pathogenic variants on VASH enzymatic activity**

We obtained whole-blood RNA from individuals from Family 1, and found no evidence that the p.Q28\* variant resulted in nonsense mediated decay (Figures S2 and S3). Hypothesizing that these protein-truncating variants would nonetheless impair the function of SVBP, we examined the ability of mouse VASH1 enzyme to dephosphorylate  $\alpha$ -tubulin in the presence of SVBP proteins either in their native form, or with the p.Q28\* and p.K13Nfs\*18 variants observed in human patients (Figure 2a). Expression of VASH in HEK293T cells alone resulted in a slight increase of dephosphorylated tubulin (due to the presence of endogenous SVBP in cells), whereas expression with native SVBP resulted in a substantial increase in dephosphorylated tubulin and a large loss of phosphorylated tubulin, thus revealing the dephosphorylation activity due to exogenous VASH-SVBP complex. When VASH was expressed with the SVBP mutants, the levels of modified tubulin did not differ from the conditions observed in the absence of SVBP (Figure 2a). This is mostly due to instability of the SVBP mutants: whereas native SVBP was easily detected, in similar experimental conditions p.Q28\* was hardly detected and p.K13Nfs\*18 could not be detected at all (see Flag signals in Figure 2a). Moreover, even the expression of the VASH was affected by the expression of the SVBP mutants (GFP signals), as expected from the known instability of the VASH in the absence of its chaperone SVBP (13, 14). Thus, the p.Q28\* and p.K13Nfs\*18 variants effectively result in a functional knockout of *SVBP*.

To investigate the function of *Svbp* *in vivo*, KO mice were produced by CRISPR/Cas9 technique. Homozygous mice, having a deletion after the third residue of SVBP generating a frameshift adding only four chimeric residues (Figure S4), were obtained by selective breeding. PCR and Sanger sequencing results confirmed the deletion of targeted region. These *Svbp* KO mice are viable, fertile, exhibited normal general development and do not exhibit weight loss compared to wild-type mice.

### **Defects in tubulin tyrosination in brain of SVBP knockout mice**

We analyzed the levels of tyrosinated, detyrosinated and  $\Delta 2$   $\alpha$ -tubulin (a modification that follows, and thus depends on, detyrosination) in the brain of *Svbp* KO mice (Figure 2 b-e). Detyrosinated and  $\Delta 2$  tubulin drastically decreased ( $-39.9 \pm 2.3$  % and  $-33.0 \pm 2.3$  %, respectively), and a 3-fold increase in tyrosinated tubulin was observed ( $+233.4 \pm 7.9\%$ ). Thus the absence of the VASH-stabilizing SVBP chaperone leads to drastic changes of  $\alpha$ -tubulin modifications, with a large reduction of tubulin detyrosination. The remaining pool of detyrosinated  $\alpha$ -tubulin could be due to  $\alpha 4$ -tubulin (which genetically lacks the C-terminal tyrosine) or to other detyrosinases (13, 14). The accumulation of tyrosinated tubulin could be the result of neosynthesis of tyrosinated tubulin that cannot be detyrosinated at specific stage of brain development.

### **SVBP-null neurons show anomalies of their differentiation and morphology.**

We then examined the three pools of  $\alpha$ -tubulin (tyrosinated, detyrosinated and  $\Delta 2$ ) in hippocampal neurons prepared from wild-type and *Svbp* KO mice brains embryos (Figure S5) cultured 2, 7 and 17 days *in vitro* (2, 7 and 17 DIV). In young neurons, the absence of SVBP leads to a drastic decrease of detyrosinated tubulin ( $-63.6 \pm 1.8$  % and  $-73.8 \pm 1.5$  % at day 2

and day 7 of DIV, respectively) and  $\Delta 2$  tubulin almost disappeared. In mature *Svbp* KO neurons (17 DIV), the decrease of detyrosinated tubulin is maintained but less pronounced ( $-37.7 \pm 11.7$  %) and  $\Delta 2$  tubulin present ( $36 \% \pm 9.1$  % of the controls). On the other hand, tyrosinated tubulin accrued extensively in the KO neurons, with a 1.5-fold increase observed at 2 DIV and a 3-fold increase observed after 7 DIV.

As in brain, the remaining pools of detyrosinated  $\alpha$ -tubulin in neurons missing SVBP (and thus vasohibin-SVBP detyrosinating activity) could be due to  $\alpha 4$ -tubulin or to other detyrosinases<sup>13,14</sup>. Yet, the notable accumulation of tyrosinated tubulin in neurons observed before 7 DIV strongly suggest that, at these early stages of neuronal differentiation, the detyrosination of large pools of  $\alpha$ -tubulin cannot be performed by other enzymes than vasohibin-SVBP complexes.

Confocal images of *Svbp* KO neurons cultured 2 DIV showed a large decrease in the amount of detyrosinated tubulin (Figure 3a) compared to wild type neurons. Remaining detyrosinated pools are concentrated in axons, whereas the other neurites exhibit tyrosinated tubulin. Moreover, SVBP deficiency led to a large decrease of neurons bearing an axon at 2 DIV (from  $55.8 \pm 4.0$  % to  $29.7 \pm 3.3$  %), revealing a clear delay in axonal differentiation (Figure 3b). *Svbp* KO neurons at 2 DIV developed an increased number of primary neurites and extra branches whereas the axon length was significantly reduced ( $-26.5 \% \pm 4.4$  %) (Figure 3c-e). At 17 DIV, after complete neuronal maturation, *Svbp* KO neurons still show a significant increase in their dendritic branching compared to wild-type neurons within the first 150  $\mu$ m close to the soma, as measured by Sholl analysis (Figure 3f).

Altogether, in neurons, SVBP deficiency resulted in marked changes in the pools of modified  $\alpha$ -tubulin and in a delay of axon differentiation associated with severe morphological defects.

## **Brain morphological defects associated with *Svbp* deletion in mice**

We performed brain imaging and morphometric assessments of wild-type and *Svbp* KO mice using anatomical MRI (Figure 4). *Svbp* KO mice show a significant decrease of the whole brain volume (7.3 %) affecting a large number of the brain regions including the cortex (7.8 %), the striatum (10.5 %), the hypothalamus (10.0 %), the thalamus (10.4 %) and the brainstem (10.0 %). We also performed measurements of white matter structures and found a strong significant reduction of several structures, for example the corpus callosum (33.7 %), the fimbria (31.7 %) and the anterior commissure (38.9 %). Thus, *Svbp* deletion in mice results in a microcephaly affecting more severely the white matter, revealing deficiencies of axonal tracts.

### **Behavioral defects associated with *Svbp* deletion in mice**

A comprehensive behavioral analysis of *Svbp* KO mice as compared to wild-type mice was performed. Firstly, we assayed locomotor activity in an open field. The total distance traveled by a mouse cumulated over 30 min was recorded. The responses exhibited by *Svbp* KO mice were enhanced compared with the wild-type (Figure 5a; WT:  $7306 \pm 464$ cm, *Svbp* KO:  $9397 \pm 595$ cm), indicating that the KO mice were more active than their wild-type counterparts.

We next evaluated cognitive abilities by investigating memory and social behavior. We monitored spontaneous alternation in a Y-maze, a test of spatial learning and memory. We found no difference between wild-type and *Svbp* KO mice in the alternation frequency (Figure S6a) indicating that the memory and willingness of KO mice to enter new environments was not affected. Social behavior was then assayed using the Resident-Intruder Test. Male mice are territorial and will react to an unfamiliar male placed in their home cage. We analyzed the behavior of a resident male, isolated either 1 or 3 weeks, when exposed to an intruder by measuring the time spent in active investigation. As shown in Figure 5b, *Svbp* KO mice exhibited a significant reduction of social investigation, compared to wild-type mice (WT:  $150.1 \pm 9.2$  s and  $142.6 \pm 12.7$  s, *Svbp* KO:  $105.3 \pm 12.6$  s and  $84.3 \pm 3.1$  s, respectively for 1

and 3 weeks of isolation). In addition, we investigated the exploratory behavior of mice in the Hamlet test (26). Animals were repeatedly trained in the apparatus and analyses of the time spent in each houses during training days showed a significant increase in the presence of *Svbp* KO mice in the Hide house, a trend to decreased presence in the Interact house and no change in the 3 other houses, Run, Eat and Drink (Figure 5d), as compared to the group of wild-type mice. Data analyzed in terms of number of entries failed to show any difference whatever the house.

In parallel, we monitored possible depressive/anxiety-like status of *Svbp* KO mice. For that we performed the Novelty Suppressed Feeding (NSF) test where the animal's motivation to eat competes with the aversive signal of bright illumination. We measured the latency to eat and found that *Svbp* KO mice behave as wild-type mice (Figure S6b). We next used the Elevated Plus Maze test, using a maze composed of two open and two enclosed arms. Mice exhibit aversion to open spaces and will remain in enclosed spaces. In this test, *Svbp* KO mice behave as wild-type mice (Figure S6c). Finally, we used the Marble Burying Test, a test based on the fact that mice will bury harmful objects in their bedding. Each mouse was introduced in a cage containing 24 marbles for 30 min, and the number of buried marbles was then counted. As shown in Figure 5c, *Svbp* KO mice buried significantly less marbles than wild-type mice (WT:  $12.77 \pm 1.2$ , *Svbp* KO:  $8.00 \pm 0.81$ ) indicating a possible lessening of anxiety and of interaction with the environment.

In summary, *Svbp* KO mice were more active than wild-type mice, do not exhibit severe memory defects, and seem to be less anxious than wild-type mice. Interestingly, they exhibit an impaired social behavior, showed by reduced interaction with the stranger mouse in the resident intruder test and a trend in the Hamlet, together with a higher time spent in the safe place provided by the Hide house in this device.

## Discussion

In this study, we initially assessed a large consanguineous Pakistani kindred (family 1) using a combination of linkage analysis and WGS, identifying a c.82C>T; p.Q28\* variant in *SVBP* as the most likely candidate. Although genetic co-segregation (Figure 1a) was confirmed in June 2012, the gene was then known as *CCDC23* and little was known about the function of the encoded 66 amino-acid protein. The variant could therefore not conclusively be confirmed to be causative for the intellectual disability, microcephaly and spasticity observed in affected family members. Although initially identified as a secretory chaperone for VASH1 and proposed to play a regulatory role in angiogenesis (18), it was the recent studies confirming *SVBP*'s importance in tubulin detyrosination and neuron differentiation (13, 14) that prompted the functional testing required to confirm this variant as the causative allele. The protein-truncating changes were associated with an absence of a catalytically active enzymatic complex VASH-SVBP, as shown by in cell-activity tests of the variants. Results from HEK293T cells were then recapitulated in the brains of KO mice, where reduced levels of detyrosinated tubulin were observed, together with concomitant increases in tyrosinated tubulin. This is the first demonstration of the link between the clinical characteristics observed in patients with *SVBP* mutations and the underlying molecular defect of tubulin detyrosination. This study also highlights the importance of reassessing clinical genomic data (27, 28).

Additional evidence supporting pathogenicity comes from our recent identification of *SVBP* mutations in two additional families, with affected individuals sharing significant phenotypic overlaps. Although we registered the phenotype and genes in the chromosome 1 linkage region from Family 1 on GeneMatcher (<https://genematcher.org/>), this genetic replication came through a more unconventional route; Family 2 was identified during a two-week trial of the CentoMD mutation database (25). Family 3 was ascertained through access to the 100K

Genomes Project; this study represents one of the first novel genes to be reported from that program.

Whilst this manuscript was in preparation, Iqbal *et al* described four individuals with intellectual disability, microcephaly, hypotonia and ataxia who were homozygous for the same p.Q28\* variant (29). Although their two kindreds were of Syrian and Pakistani ethnicity, a single ancestral disease haplotype of 1.8 Mb was shared across both families. Where a genotype-phenotype relationship is based on a single disease haplotype, caution should be exercised as it is possible that an unobserved pathogenic mutation may lie on the same haplotype as the candidate variant (30, 31). Without WGS data, it is difficult to exclude the possibility that a rare non-coding variant or a cryptic structural variant could have been missed. In contrast, we have WGS data for both families harboring the p.Q28\* disease haplotype and the uniformity of coverage means we are better able to exclude such scenarios. The genotype-phenotype correlation is further corroborated by the results for Family 2 where a different truncating *SVBP* variant was detected in patients exhibiting the same phenotype.

Detailed phenotypic descriptions of the 8 affected individuals described here allows us to start to delineate the range of phenotypic features associated with defective detyrosination in humans. In combination with the 4 patients reported by Iqbal *et al* (29), it is clear that the disorder comprises several common features as well as a number of variable characteristics. All patients presented with intellectual disability (moderate to profound), delayed speech and delayed gross motor development. Microcephaly was another common feature in human patients and this mirrors what was observed in *Svbp* KO mice where there was a 7% loss in global brain volume. Neuroradiological assessment of human MRI data (Figure 1 d,e) highlighted consistent albeit subtle features including enlarged ventricles and a thin corpus callosum. Notably in KO mice this last brain region was also reduced by 33.7%. The most conspicuous difference between the families described here and those reported by Iqbal *et al*

(29) is that the previous group of patients were all reported to have hypotonia, whereas the majority of patients we identified had increased muscle tone, predominantly in the lower limbs. Other variable features observed multiple times in our case series include digital abnormalities, mirror movements, coarse facial features and infantile seizures. Iqbal and colleagues reported chest abnormalities in 2 of their 4 patients but this feature was not noted in our families. Behavioral characteristics may include aggression, described in two patients (29) and autism, described in one patient reported here. Although behavioral traits are difficult to model in rodents, we note that the *Svbp* KO mice in this study also exhibited a significant reduction of social investigation and possibly lower levels of anxiety associated with a low interest for their physical environment.

The tubulin tyrosination/detyrosination cycle is one of several post-translational modifications of neuronal tubulin. Other modifications include acetylation, polyglycylation and polyglutamylation, and collectively these are known as the “tubulin code”. Over the last decade, studies in mice have linked tubulin acetylation and polyglutamylation to neurodegeneration (32-35). More recently, a causal relationship between the CCP1 deglutamylase and neurodegeneration was found in humans (36). CCP1 deglutamylase is responsible for the successive removal of the two glutamate amino acids immediately preceding the C-terminal tyrosine, yielding  $\Delta 2$ - and  $\Delta 3$ - $\alpha$ -tubulin (37). Detyrosinated  $\alpha$ -tubulin is a substrate for the CCP1 enzyme and so it is not surprising that decreased levels  $\Delta 2$ - $\alpha$ -tubulin were observed in brains of the *Svbp* KO mice (Fig 2 b,e). Whilst the patients described in the present study did not show signs of cerebellar atrophy, shared features seen in both SVBP and CCP1 patient cohorts include microcephaly, hypotonia, spasticity, developmental delay and corpus callosum dysplasia.

The most frequent form of hereditary spastic paraplegia is caused by mutations in *SPAST* (38). *SPAST* encodes an enzyme that shows microtubule-severing activity, a process

which in turn is regulated by tubulin glutamylation (39), another type of post-translational modification that is common in mammalian brain tissue. It is also worth noting that detyrosinated microtubules are known to play a role in modulation of mechanotransduction in muscle (40). It is therefore unsurprising that the abnormal phenotype seen in patients included muscular component and in most cases this was in the form of lower limb spastic paraparesis. Interestingly, this feature was not recapitulated in the *Svbp* KO mouse model, where the open field locomotor activity was demonstrated to be increased.

The present study is the first detailed description of *Svbp* KO mice. Anatomical MRI indicates microcephaly and this whole brain volume reduction affects all brain structures analyzed. The brain size reduction is not associated with a general loss of body weight, indicating a specific alteration. *Svbp* deletion results in a severe reduction of the white matter with both intra-hemispheric (corpus callosum) and cortical tracts (fimbria, anterior commissure) defects.

The observed reduction of brain volume most possibly originates from an abnormal differentiation and maturation of deficient neurons. In agreement, *Svbp* KO cultured neurons showed a clear delay of their axon differentiation and severe morphological defects. Moreover, downregulation of SVBP was shown to disrupt neuronal migration in developing mouse neocortex (13). Anomalies of progenitor proliferation might also occur since VASH-SVBP complexes were recently shown to be critical during mitosis (41). Finally, the reduction of brain volume might also involve a reduction of synapse density, as suggested by shRNA knockdown experiments in rat hippocampal neurons (29). A whole *in vivo* analysis of neurons morphology and spines integrity will be needed to obtain a full picture of synaptic functioning in the absence of SVBP. Altogether our work clearly indicates that *Svbp* deletion results in brain defects more probably originating from neurodevelopmental anomalies. VASH-SVBP complexes are major regulators of detyrosination and thus of microtubule dynamics in neuronal cells (13, 17). The

defects linked to *Svbp* deletion reported in this work highlight the importance of microtubules integrity for brain homeostasis and support the view that microtubule dysfunction can lead to neurodevelopmental disorders and neurodegeneration.

The comprehensive behavioral analysis of *Svbp* KO mice indicates several abnormal parameters. *Svbp* KO mice exhibit an enhanced locomotor sensitivity reaction when exposed to novelty. The possible anxious state of the mutant mice was investigated using the Marble Burying Test and the Elevated Plus Maze, however these results were difficult to interpret. *Svbp* KO mice showed no anxious behavior in the Elevated + Maze, whereas they buried a substantially lower number of marbles than wild-type mice in the Marble Test, possibly indicative of a low anxious state. This latter defect might rather be attributed to a lower interest for their environment. This result is in agreement with (a) the reduced interest of SVBP mice for their congener observed in the resident intruder test, and (b) the results of the Hamlet test. Indeed, training of the animals in this complex environment providing distinct functionalized spots for eating, drinking, running, hiding and interacting identified only two differences in the *Svbp* KO mice behavior as compared with wild-type littermates, namely a trend to decrease interaction with the stranger mouse and a significant increase of time spent in the tunnel of the Hide house. Assessment of intellectual disability related defects in mice often relies on analysis of the working memory. *Svbp* KO mice do not exhibit deficit in Y-maze test which relies on measuring memory related to spatial exploration while factors such as motivational or emotional states are minimized and in which learning a rule is not involved. This result suggests that the working memory *per se* is not affected by *Svbp* deletion.

In summary, we have shown that rare biallelic variants in *SVBP* result in loss of tubulin deetyrosination activity, causing anatomical brain deficits associated with intellectual disability. The three families we describe have several features which are recapitulated in the KO mouse model, which is described here for the first time. This study thus adds to the growing list of

471 diseases linked to aberrant microtubule cytoskeleton and point to the importance of microtubule  
472 dynamics.  
473

## **Materials and methods**

### **Whole-genome or whole-exome sequencing and variant filtering**

Appropriate informed consent was obtained for all human subjects.

#### **Family 1**

Individual V-6 from family 1 underwent WGS in December 2011 using a HiSeq2000 machine (Illumina) and v3 chemistry, as part of the WGS500 project. Further details of the sequencing, read alignment and variant calling have been described previously (42). The proband's unaffected mother (IV-2), affected sister (V-7) and affected uncle and aunt (IV-3 and IV-4) were genotyped on either the Illumina CytoSNP12 or the OmniExpress microarray (Figure 1a). Since the parents of both pairs of affected siblings were first cousins, we considered the simple recessive model most likely, so focused on regions that were identical-by-descent for both alleles (IBD2) and homozygous in all the affected individuals. However, a compound recessive model would also fit the pedigree, and so we also considered regions that were IBD2 and heterozygous. To identify these regions, we selected SNV markers for linkage with linkdatagen (43) and then ran MERLIN (44) using the Kong and Cox exponential model (45), specifying a recessive model.

We then searched for rare coding variants within the linked regions. We excluded variants with a frequency greater than 0.5% in the 1000 Genomes project (46), the NHLBI Exome Sequencing project (<http://evs.gs.washington.edu/EVS/>), gnomAD, or in our own WGS500 project (42), and those that were seen as homozygotes in any of these projects (other than in individual V-6). We also prioritized variants in regions that were highly conserved across the 46 vertebrate species in the UCSC conservation track. Candidate variants were genotyped in the other unaffected siblings by Sanger sequencing to check segregation. Since there was insufficient evidence based on the WGS500 project to implicate a pathogenic variant in these patients' condition the family were later recruited to the 100,000 Genomes

Project (<https://doi.org/10.6084/m9.figshare.4530893.v4>), a national project that aims to establish the use of WGS in the National Health Service and which has been described in detail elsewhere (47). Reads were mapped to GRCh37 using the Isaac aligner and variants were called using the Isaac variant caller (Illumina). Structural variants were called with Manta and Canvas (Illumina). As part of this study, samples were also genotyped using the InfiniumCoreExome-24v1 array (Illumina).

### **Families 2 and 3**

The affected proband (II-3) from family 2 and her parents underwent WES analysis at CentoGene. WES workflows and results from the 1000 families were described previously (48). Results for family 2 were incorporated into the searchable CentoMD mutation database (CentoGene, [www.centogene.com/pharma/mutation-database-centomd.html](http://www.centogene.com/pharma/mutation-database-centomd.html)) (25).

Family 3 were whole-genome sequenced as a quad, as part of the 100,000 Genomes Project (as described above). Samples were also genotyped using the InfiniumCoreExome-24v1 array (Illumina). Family 3 was identified from the rare disease subgroup of the 100,000 Genomes Project using a customized bcftools script designed to search through vcf.gz files specifically looking for loss of function (LoF) variants in *SVBP*. Genotypes from WGS and from the InfiniumCoreExome-24v1 arrays were used to assess identity by descent sharing across chromosome 1 by looking for extended regions sharing identical genotype calls.

### ***In cellulo* tubulin detyrosination assay**

A plasmid encoding mouse SVBP (NM\_024462) with C-terminal myc and Flag tags (SVBP-myc-Flag) was obtained from OriGene (MR200054). Using this plasmid we deleted residues 28-66 (mimicking p.Q28\*) or replaced residues 13-66 by the 17 residues resulting from the frameshift p.K13Nfs\*18. Mouse Vash1 cDNA (NM\_177354) was PCR-amplified from

plasmid Vash1-myc-DDK (Origin, MR222250) and inserted into pEGFP-N1 vector (Clontech), to generate vasohibin-1 with EGFP fused to its C-terminus (V1-GFP). All plasmids were verified for sequence integrity.

HEK293T cells were maintained under standard conditions and were transfected using JetPEI transfection reagent (Polyplus-Transfection). A ratio of 1:1 was used for cDNA co-transfections (for VASH1 with SVBP, and with variants). Protein extracts from HEK293T cells were prepared directly by scraping the cell layer in Laemmli buffer.

### **Generation of *Svbp* KO mice**

The *Svbp* mutation was generated by CRISPR/Cas9 editing. Guide selection and off-target predictions were made with CRISPOR software (49). Exon 2 target sequence (GATTTTCTTTCCGGGCAGG) was unique in the genome. Predicted off-target sequences on the same chromosome were all non exonic, and with at least 4 mismatches (partly localized close to the PAM) with on-target sequences. A dual guide RNA was prepared by combining synthetic tracrRNA (TriLink BioTechnologies) and crRNA (Eurogentec, Angers, France). Sequences are given in Table S2. A cloning free procedure (50) was used to modify the *Svbp* locus, by microinjection of Cas9/RNA complexes into *in vitro* fertilized B6D2F1xFVB embryos. F0 mosaic animals born after reimplantation of microinjected embryos were genotyped by PCR and Sanger sequencing, and then mated to C57BL/6 mice to provide F1 founder mice. Among these, a mouse was selected for the frameshift introducing as few extra amino acids as possible after the third amino-acid of SVBP. The allele was designated *Svbp*P4Rfs\*6 and the corresponding protein sequence is MDPRKIQS (extra amino-acids in italics). At least 8 additional back-crosses were performed with C57BL/6 mice before phenotyping in order to avoid possible confounding effects due to off-target mutations. The study protocol was approved by the local animal welfare committee (Comité Local Grenoble

Institute Neurosciences, C2EA-04) and complied with EU guidelines (directive 2010/63/EU). Every precaution was taken to minimize stress and the number of animals used in each experiment. All experiments were conducted on wild-type and *Svbp* KO adult (3-6 months) littermates with a C57BL/6 genetic background.

## **Antibodies**

Tyrosinated, detyrosinated and  $\Delta 2$   $\alpha$ -tubulin were detected in cells and tissues by immunoblots using specific antibodies, as described previously (37). The other primary antibodies used were as follows: rabbit anti-Flag from Molecular Probes (1:10,000), rabbit anti-GFP from Chromotek (1:5,000), rabbit anti-GAPDH from Sigma (1:10,000).

## **Immunoblot analysis of $\alpha$ -tubulin variants in neuron and brain protein extracts**

For neurons protein extracts analysis, cells were collected after 2, 7 or 17 DIV. After washing with phosphate-buffered saline (PBS) medium at 37°C, neurons were directly lysed in Laemmli buffer.

For analysis of mice tissues, crude protein extracts were prepared using a FastPrep Instrument (MP Biomedicals, Illkirch, France). Brain proteins were extracted in 100 mM 1,4-piperazinediethanesulfonic acid at pH 6.7, 1 mM EGTA, 1 mM MgCl<sub>2</sub>, and protease inhibitors (Complete Mini EDTA-free; Roche Diagnostics, Meylan, France). Cell remnants were eliminated by a 10 min centrifugation at 10,000  $\times$  g, and Laemmli buffer was added to the supernatant.

Protein extracts were then loaded on 10% acrylamide gels (Mini-PROTEAN® TGX Stain-Free™, Biorad) and transferred with Trans-Blot® Turbo (BioRad). Membranes were incubated with primary antibodies, with secondary antibodies conjugated with HRP (1:10 000, from Jackson ImmunoResearch), and finally revealed with Chemidoc camera (Biorad). For

analysis and graphical representations of immunoblots (Fig. 3b,c and S6c), protein bands were quantified from triplicate blots of 3 different experiments using Image Lab software (Bio-Rad). Tyrosinated, detyrosinated or  $\Delta 2$   $\alpha$ -tubulin signals were normalized to the protein content of the sample estimated from its GAPDH signal.

### **Neuronal cultures and morphometric analysis**

Hippocampal neurons were cultured from E17.5 WT or *Svbp* KO embryos as described (12).

For axonal and neurite morphometric analysis, neurons were fixed after 2 DIV, immunolabeled and analyzed as previously described (13). 20 neurons per embryo, from 6 different WT or *Svbp* KO embryos were analyzed.

For Sholl analysis, 1% of cultured hippocampal neurons were infected with 30 MOI of a lentivirus containing GFP (pWPT-GFP addgene.org/12255) and plated onto a monolayer of non-infected neurons. After 17 DIV, neurons were fixed and images were taken with an 20x/0.5 objective with an inverted Nikon microscope equipped with a camera EMCCD (Coolsnap, photometrics) piloted by Metaview software. Images were processed by the Tubeness filter, thresholded and converted to mask. Final masks were analyzed using the Sholl Analysis plugin of ImageJ. 15 to 20 neurons per embryo, from 4 WT and 3 *Svbp* KO embryos were analyzed.

### **Brain preparation for *ex vivo* MRI acquisitions**

Brains were prepared as previously described (51). Briefly, brains were fixed before harvesting from animals by a transcardiac perfusion of a 4% paraformaldehyde solution in phosphate buffered saline added with a MRI contrast agent (6.25 mM of Gd-DOTA; Guerbet Laboratories, Roissy, France). The contrast agent was used here to reduce MRI acquisition time. After removing surrounding skin and muscles, the skulls containing intact brains were immersed in the fixing solution for four days, and then transferred to a Fomblin (FenS chemicals, Goes,

Netherlands) bath for at least seven days after brain fixation. This schedule provided homogeneous distribution of the Gd-DOTA throughout the whole brain (52).

## **MRI acquisitions**

*Ex vivo* 3D MRI acquisitions with a high spatial resolution were performed at 9.4 T (Bruker Biospec Avance III; IRMaGe facility) using a volume coil for transmission and a head surface cryocoil for reception. A 3D T<sub>1w</sub> gradient-echo MRI sequence was used for brain segmentation and volumetric analysis (repetition time: 35.2 ms, echo time: 8.5 ms, flip angle: 20°, field of view: 12 · 9 · 16 mm<sup>3</sup>, isotropic spatial resolution: 50 µm, 4 signal accumulations, total acquisition time per brain: 2 h 32 min).

## **Quantitative analysis of brain volumes**

Brain regions were defined by MRI segmentation on the 3D T<sub>1w</sub> MR images. Each cerebral structure was manually delimited using regions of interest (ROI) drawn every five slices on the coronal orientation of the 3D T<sub>1w</sub> MRI, using Fiji software (53). Using the Segmentation editor plug-in ([http://fiji.sc/Segmentation\\_Editor](http://fiji.sc/Segmentation_Editor)) the whole cerebral structure was reconstructed by interpolation between ROIs. Then, all ROIs were manually corrected based on the Allen mouse brain atlas (<http://atlas.brain-map.org/atlas>). Measurements were obtained for the following structures: the anterior commissure (ac), the brainstem (BS), the caudate putamen (CPU), the cerebellum (CB), the colliculi (CO), the corpus callosum (cc) the cortex (CX), the fimbria (fi), the globus pallidus (GP), the hippocampal formation (HF), the hypothalamus (HP), the olfactory bulb (OB) and the thalamus (TH). Each structure was color-coded, and its 3D representation and volume were determined using the 3D viewer plug-in in the Fiji software ([https://imagej.net/3D\\_Viewer](https://imagej.net/3D_Viewer)). For each region, the volume was calculated as the number of

voxels  $\times$  the voxel volume. All segmentations were done blind to the genotype. All data passed the normality test (except the BS for WT), we thus used a student t-test for group comparison.

## **Behavioral tests**

**Open Field:** Locomotor activity of mice was video-recorded via a camera mounted above an open field and connected to a computer. Horizontal activity was analyzed using Ethovision XT14 software (Noldus, Wageningen, Netherlands). In the open field condition, the activity of four mice was simultaneously monitored in a white arena (L50 x 150 x h45 cm) for 30 min. Within each genotype, mice were randomly placed in the different arenas.

The Marble Burying Test was performed as described previously (54). More precisely, the mouse was placed in a clear plastic box (L42  $\times$  126  $\times$  h15 cm), containing 24 glass marbles (1.6 cm in diameter) evenly spaced (six rows of four marbles) on 4 cm of litter. Thirty minutes later, the animals were removed from the cages, and the number of marbles buried more than two thirds in the litter was scored.

**Resident-Intruder Test:** home-cage social interaction was assessed, as described (55). The duration of sniffing investigation displayed by a resident male mouse in response to presentation of an intruder male mouse was measured. In this test, wild-type and *Svbp* KO mice were housed individually during 1 or 3 weeks prior to testing to allow establishment of a home-cage territory. The intruder mice, housed in groups, were unfamiliar to the resident mouse. In each trial, an intruder was placed in a corner of the resident home-cage (L36  $\times$  120  $\times$  h14 cm), and the exploration activity of the resident was video-recorded for 5 minutes. The time spent sniffing in close contact with the intruder was measured manually from video recordings.

The Hamlet test is a novel complex environment device that allows mice to be trained in groups in a more ecological space than the housing cage (26). The maze (160 cm diameter) is composed of a central place, streets expanding from it in a star shape and 5 houses that have

been functionalized. The houses contained a food dispenser (physiological function encoded: Eat), two water dispensers (Drink), a novomaze<sup>®</sup> (Viewpoint, Lissieu, France) (Hide), a running wheel (Run) or a compartment for a stranger mouse (Interact). Animals were placed in the Hamlet in groups of 7 from the same housing cage, for 4 h per day during a 2-weeks training period. The videotracking system (Viewpoint) recorded activity in each house in terms of number of entries and duration of presence.

## **Supplemental data**

Supplemental data includes additional methods, six figures and two tables.

## **Acknowledgments**

We thank the in vivo experimental platform, the IRMaGE platform and the zootechnicians of the Grenoble Institute Neuroscience (GIN). We also thank Cyrielle Kint ([www.diploid.com](http://www.diploid.com)) and Christian Beetz ([www.centogene.com](http://www.centogene.com)) for reviewing exome data and helping facilitate international collaboration efforts and Gerardine Quaghebeur for reviewing MRI images for family 1.

## **Conflict of Interest statement**

P.B. is Chief Scientific Officer of Centogene AG. Other authors declare no competing interests.

## **Funding**

This work was supported by the Wellcome Trust (203141/Z/16/Z) and the NIHR Biomedical Research Centre Oxford. Additional funding for the WGS500 project was from Illumina. This research was also made possible through access to the data and findings generated by the

100,000 Genomes Project. The 100,000 Genomes Project is managed by Genomics England Limited (a wholly owned company of the Department of Health). The 100,000 Genomes Project is funded by the National Institute for Health Research and NHS England. The Wellcome Trust, Cancer Research UK and the Medical Research Council have also funded research infrastructure. The 100,000 Genomes Project uses data provided by patients and collected by the National Health Service as part of their care and support. This work was also supported by grants from INSERM, University Grenoble Alpes, CNRS, CEA, La Ligue Contre le Cancer comité de l'Isère (to MJM), and fondation France Alzheimer (to MJM). The MRI facility IRMaGe is partly funded by the French program "Investissements d'Avenir" run by the French National Research Agency, grant "Infrastructure d'avenir en Biologie Santé" [ANR-11-INBS-0006].

## References

- 1 Chakraborti, S., Natarajan, K., Curiel, J., Janke, C. and Liu, J. (2016) The emerging role of the tubulin code: From the tubulin molecule to neuronal function and disease. *Cytoskeleton (Hoboken)*, **73**, 521-550.
- 2 Romaniello, R., Arrigoni, F., Bassi, M.T. and Borgatti, R. (2015) Mutations in alpha- and beta-tubulin encoding genes: implications in brain malformations. *Brain Dev*, **37**, 273-280.
- 3 Jaglin, X.H. and Chelly, J. (2009) Tubulin-related cortical dysgeneses: microtubule dysfunction underlying neuronal migration defects. *Trends Genet*, **25**, 555-566.
- 4 Jaglin, X.H., Poirier, K., Saillour, Y., Buhler, E., Tian, G., Bahi-Buisson, N., Fallet-Bianco, C., Phan-Dinh-Tuy, F., Kong, X.P., Bomont, P. *et al.* (2009) Mutations in the beta-tubulin gene TUBB2B result in asymmetrical polymicrogyria. *Nat Genet*, **41**, 746-752.
- 5 Keays, D.A., Tian, G., Poirier, K., Huang, G.J., Siebold, C., Cleak, J., Oliver, P.L., Fray, M., Harvey, R.J., Molnar, Z. *et al.* (2007) Mutations in alpha-tubulin cause abnormal neuronal migration in mice and lissencephaly in humans. *Cell*, **128**, 45-57.
- 6 Poirier, K., Keays, D.A., Francis, F., Saillour, Y., Bahi, N., Manouvrier, S., Fallet-Bianco, C., Pasquier, L., Toutain, A., Tuy, F.P. *et al.* (2007) Large spectrum of lissencephaly and pachygyria phenotypes resulting from de novo missense mutations in tubulin alpha 1A (TUBA1A). *Hum Mutat*, **28**, 1055-1064.
- 7 Kuijpers, M. and Hoogenraad, C.C. (2011) Centrosomes, microtubules and neuronal development. *Mol Cell Neurosci*, **48**, 349-358.
- 8 Walters, G.B., Gustafsson, O., Sveinbjornsson, G., Eiriksdottir, V.K., Agustsdottir, A.B., Jonsdottir, G.A., Steinberg, S., Gunnarsson, A.F., Magnusson, M.I., Unnsteinsdottir, U. *et al.* (2018) MAP1B mutations cause intellectual disability and extensive white matter deficit. *Nat Commun*, **9**, 3456.

- 9 Geuens, G., Gundersen, G.G., Nuydens, R., Cornelissen, F., Bulinski, J.C. and DeBrabander, M. (1986) Ultrastructural colocalization of tyrosinated and detyrosinated alpha-tubulin in interphase and mitotic cells. *J Cell Biol*, **103**, 1883-1893.
- 10 Gundersen, G.G. and Bulinski, J.C. (1986) Microtubule arrays in differentiated cells contain elevated levels of a post-translationally modified form of tubulin. *Eur J Cell Biol*, **42**, 288-294.
- 11 Ersfeld, K., Wehland, J., Plessmann, U., Dodemont, H., Gerke, V. and Weber, K. (1993) Characterization of the tubulin-tyrosine ligase. *J Cell Biol*, **120**, 725-732.
- 12 Erck, C., Peris, L., Andrieux, A., Meissirel, C., Gruber, A.D., Vernet, M., Schweitzer, A., Saoudi, Y., Pointu, H., Bosc, C. *et al.* (2005) A vital role of tubulin-tyrosine-ligase for neuronal organization. *Proc Natl Acad Sci U S A*, **102**, 7853-7858.
- 13 Aillaud, C., Bosc, C., Peris, L., Bosson, A., Heemeryck, P., Van Dijk, J., Le Fric, J., Boulan, B., Vossier, F., Sanman, L.E. *et al.* (2017) Vasohibins/SVBP are tubulin carboxypeptidases (TCPs) that regulate neuron differentiation. *Science*, **358**, 1448-1453.
- 14 Nieuwenhuis, J., Adamopoulos, A., Bleijerveld, O.B., Mazouzi, A., Stickel, E., Celie, P., Altelaar, M., Knipscheer, P., Perrakis, A., Blomen, V.A. *et al.* (2017) Vasohibins encode tubulin detyrosinating activity. *Science*, **358**, 1453-1456.
- 15 Adamopoulos, A., Landskron, L., Heidebrecht, T., Tsakou, F., Bleijerveld, O.B., Altelaar, M., Nieuwenhuis, J., Celie, P.H.N., Brummelkamp, T.R. and Perrakis, A. (2019) Crystal structure of the tubulin tyrosine carboxypeptidase complex VASH1-SVBP. *Nat Struct Mol Biol*, **26**, 567-570.
- 16 Li, F., Hu, Y., Qi, S., Luo, X. and Yu, H. (2019) Structural basis of tubulin detyrosination by vasohibins. *Nat Struct Mol Biol*, **26**, 583-591.
- 17 Wang, N., Bosc, C., Ryul Choi, S., Boulan, B., Peris, L., Olieric, N., Bao, H., Krichen, F., Chen, L., Andrieux, A. *et al.* (2019) Structural basis of tubulin detyrosination by the vasohibin-SVBP enzyme complex. *Nat Struct Mol Biol*, **26**, 571-582.
- 18 Suzuki, Y., Kobayashi, M., Miyashita, H., Ohta, H., Sonoda, H. and Sato, Y. (2010) Isolation of a small vasohibin-binding protein (SVBP) and its role in vasohibin secretion. *J Cell Sci*, **123**, 3094-3101.
- 19 Gumy, L.F., Chew, D.J., Tortosa, E., Katrukha, E.A., Kapitein, L.C., Tolkovsky, A.M., Hoogenraad, C.C. and Fawcett, J.W. (2013) The kinesin-2 family member KIF3C regulates microtubule dynamics and is required for axon growth and regeneration. *J Neurosci*, **33**, 11329-11345.
- 20 Hammond, J.W., Huang, C.F., Kaech, S., Jacobson, C., Banker, G. and Verhey, K.J. (2010) Posttranslational modifications of tubulin and the polarized transport of kinesin-1 in neurons. *Mol Biol Cell*, **21**, 572-583.
- 21 Kahn, O.I., Sharma, V., Gonzalez-Billault, C. and Baas, P.W. (2015) Effects of kinesin-5 inhibition on dendritic architecture and microtubule organization. *Mol Biol Cell*, **26**, 66-77.
- 22 Konishi, Y. and Setou, M. (2009) Tubulin tyrosination navigates the kinesin-1 motor domain to axons. *Nat Neurosci*, **12**, 559-567.
- 23 Marcos, S., Moreau, J., Backer, S., Job, D., Andrieux, A. and Bloch-Gallego, E. (2009) Tubulin tyrosination is required for the proper organization and pathfinding of the growth cone. *PLoS One*, **4**, e5405.
- 24 Nirschl, J.J., Magiera, M.M., Lazarus, J.E., Janke, C. and Holzbaur, E.L. (2016) alpha-Tubulin Tyrosination and CLIP-170 Phosphorylation Regulate the Initiation of Dynein-Driven Transport in Neurons. *Cell Rep*, **14**, 2637-2652.
- 25 Trujillano, D., Oprea, G.E., Schmitz, Y., Bertoli-Avella, A.M., Abou Jamra, R. and Rolfs, A. (2017) A comprehensive global genotype-phenotype database for rare diseases. *Mol Genet Genomic Med*, **5**, 66-75.
- 26 Crouzier, L., Gilabert, D., Rossel, M., Trousse, F. and Maurice, T. (2018) Topographical memory analyzed in mice using the Hamlet test, a novel complex maze. *Neurobiol Learn Mem*, **149**, 118-134.
- 27 Eldomery, M.K., Coban-Akdemir, Z., Harel, T., Rosenfeld, J.A., Gambin, T., Stray-Pedersen, A., Kury, S., Mercier, S., Lessel, D., Denecke, J. *et al.* (2017) Lessons learned from additional research analyses of unsolved clinical exome cases. *Genome Med*, **9**, 26.
- 28 Wright, C.F., McRae, J.F., Clayton, S., Gallone, G., Aitken, S., FitzGerald, T.W., Jones, P., Prigmore, E., Rajan, D., Lord, J. *et al.* (2018) Making new genetic diagnoses with old data: iterative

reanalysis and reporting from genome-wide data in 1,133 families with developmental disorders. *Genet Med*, **20**, 1216-1223.

29 Iqbal, Z., Tawamie, H., Ba, W., Reis, A., Halak, B.A., Sticht, H., Uebe, S., Kasri, N.N., Riazuddin, S., van Bokhoven, H. *et al.* (2019) Loss of function of SVBP leads to autosomal recessive intellectual disability, microcephaly, ataxia, and hypotonia. *Genet Med*, in press.

30 Karaca, E., Posey, J.E., Coban Akdemir, Z., Pehlivan, D., Harel, T., Jhangiani, S.N., Bayram, Y., Song, X., Bahrambeigi, V., Yuregir, O.O. *et al.* (2018) Phenotypic expansion illuminates multilocus pathogenic variation. *Genet Med*, **20**, 1528-1537.

31 MacArthur, D.G., Manolio, T.A., Dimmock, D.P., Rehm, H.L., Shendure, J., Abecasis, G.R., Adams, D.R., Altman, R.B., Antonarakis, S.E., Ashley, E.A. *et al.* (2014) Guidelines for investigating causality of sequence variants in human disease. *Nature*, **508**, 469-476.

32 Dompierre, J.P., Godin, J.D., Charrin, B.C., Cordelieres, F.P., King, S.J., Humbert, S. and Saudou, F. (2007) Histone deacetylase 6 inhibition compensates for the transport deficit in Huntington's disease by increasing tubulin acetylation. *J Neurosci*, **27**, 3571-3583.

33 Magiera, M.M., Bodakuntla, S., Ziak, J., Lacomme, S., Marques Sousa, P., Leboucher, S., Hausrat, T.J., Bosc, C., Andrieux, A., Kneussel, M. *et al.* (2018) Excessive tubulin polyglutamylation causes neurodegeneration and perturbs neuronal transport. *EMBO J*, **37**, 1-14.

34 Outeiro, T.F., Kontopoulos, E., Altmann, S.M., Kufareva, I., Strathearn, K.E., Amore, A.M., Volk, C.B., Maxwell, M.M., Rochet, J.C., McLean, P.J. *et al.* (2007) Sirtuin 2 inhibitors rescue alpha-synuclein-mediated toxicity in models of Parkinson's disease. *Science*, **317**, 516-519.

35 Rogowski, K., van Dijk, J., Magiera, M.M., Bosc, C., Deloulme, J.C., Bosson, A., Peris, L., Gold, N.D., Lacroix, B., Bosch Grau, M. *et al.* (2010) A family of protein-deglutamylating enzymes associated with neurodegeneration. *Cell*, **143**, 564-578.

36 Shashi, V., Magiera, M.M., Klein, D., Zaki, M., Schoch, K., Rudnik-Schoneborn, S., Norman, A., Lopes Abath Neto, O., Dusl, M., Yuan, X. *et al.* (2018) Loss of tubulin deglutamylase CCP1 causes infantile-onset neurodegeneration. *EMBO J*, **37**, 1-12.

37 Aillaud, C., Bosc, C., Saoudi, Y., Denarier, E., Peris, L., Sago, L., Taulet, N., Cieren, A., Tort, O., Magiera, M.M. *et al.* (2016) Evidence for new C-terminally truncated variants of alpha- and beta-tubulins. *Mol Biol Cell*, **27**, 640-653.

38 Tarrade, A., Fassier, C., Courageot, S., Charvin, D., Vitte, J., Peris, L., Thorel, A., Mouisel, E., Fonknechten, N., Roblot, N. *et al.* (2006) A mutation of spastin is responsible for swellings and impairment of transport in a region of axon characterized by changes in microtubule composition. *Hum Mol Genet*, **15**, 3544-3558.

39 Valenstein, M.L. and Roll-Mecak, A. (2016) Graded Control of Microtubule Severing by Tubulin Glutamylation. *Cell*, **164**, 911-921.

40 Kerr, J.P., Robison, P., Shi, G., Bogush, A.I., Kempema, A.M., Hexum, J.K., Becerra, N., Harki, D.A., Martin, S.S., Raiteri, R. *et al.* (2015) Detyrosinated microtubules modulate mechanotransduction in heart and skeletal muscle. *Nat Commun*, **6**, 8526.

41 Liao, S., Rajendraprasad, G., Wang, N., Eibes, S., Gao, J., Yu, H., Wu, G., Tu, X., Huang, H., Barisic, M. *et al.* (2019) Molecular basis of vasohibins-mediated detyrosination and its impact on spindle function and mitosis. *Cell Res*, **29**, 533-547.

42 Taylor, J.C., Martin, H.C., Lise, S., Broxholme, J., Cazier, J.B., Rimmer, A., Kanapin, A., Lunter, G., Fiddy, S., Allan, C. *et al.* (2015) Factors influencing success of clinical genome sequencing across a broad spectrum of disorders. *Nat Genet*, **47**, 717-726.

43 Bahlo, M. and Bromhead, C.J. (2009) Generating linkage mapping files from Affymetrix SNP chip data. *Bioinformatics*, **25**, 1961-1962.

44 Abecasis, G.R., Cherny, S.S., Cookson, W.O. and Cardon, L.R. (2002) Merlin--rapid analysis of dense genetic maps using sparse gene flow trees. *Nat Genet*, **30**, 97-101.

45 Kong, A. and Cox, N.J. (1997) Allele-sharing models: LOD scores and accurate linkage tests. *Am J Hum Genet*, **61**, 1179-1188.

- 46 Genomes Project, C., Auton, A., Brooks, L.D., Durbin, R.M., Garrison, E.P., Kang, H.M., Korbel, J.O., Marchini, J.L., McCarthy, S., McVean, G.A. *et al.* (2015) A global reference for human genetic variation. *Nature*, **526**, 68-74.
- 47 Turnbull, C., Scott, R.H., Thomas, E., Jones, L., Murugaesu, N., Pretty, F.B., Halai, D., Baple, E., Craig, C., Hamblin, A. *et al.* (2018) The 100 000 Genomes Project: bringing whole genome sequencing to the NHS. *BMJ*, **361**, k1687.
- 48 Trujillano, D., Bertoli-Avella, A.M., Kumar Kandaswamy, K., Weiss, M.E., Koster, J., Marais, A., Paknia, O., Schroder, R., Garcia-Aznar, J.M., Werber, M. *et al.* (2017) Clinical exome sequencing: results from 2819 samples reflecting 1000 families. *Eur J Hum Genet*, **25**, 176-182.
- 49 Haeussler, M., Schonig, K., Eckert, H., Eschstruth, A., Mianne, J., Renaud, J.B., Schneider-Maunoury, S., Shkumatava, A., Teboul, L., Kent, J. *et al.* (2016) Evaluation of off-target and on-target scoring algorithms and integration into the guide RNA selection tool CRISPOR. *Genome Biol*, **17**, 148.
- 50 Teixeira, M., Py, B.F., Bosc, C., Laubret, D., Moutin, M.J., Marvel, J., Flamant, F. and Markossian, S. (2018) Electroporation of mice zygotes with dual guide RNA/Cas9 complexes for simple and efficient cloning-free genome editing. *Sci Rep*, **8**, 474.
- 51 Gimenez, U., Boulan, B., Mauconduit, F., Taurel, F., Leclercq, M., Denarier, E., Brocard, J., Gory-Faure, S., Andrieux, A., Lahrech, H. *et al.* (2017) 3D imaging of the brain morphology and connectivity defects in a model of psychiatric disorders: MAP6-KO mice. *Sci Rep*, **7**, 10308.
- 52 Gimenez, U., Perles-Barbacaru, A.T., Millet, A., Appaix, F., El-Atifi, M., Pernet-Gallay, K., van der Sanden, B., Berger, F. and Lahrech, H. (2016) Microscopic DTI accurately identifies early glioma cell migration: correlation with multimodal imaging in a new glioma stem cell model. *NMR Biomed*, **29**, 1553-1562.
- 53 Schindelin, J., Arganda-Carreras, I., Frise, E., Kaynig, V., Longair, M., Pietzsch, T., Preibisch, S., Rueden, C., Saalfeld, S., Schmid, B. *et al.* (2012) Fiji: an open-source platform for biological-image analysis. *Nat Methods*, **9**, 676-682.
- 54 Delotterie, D., Ruiz, G., Brocard, J., Schweitzer, A., Roucard, C., Roche, Y., Suaud-Chagny, M.F., Bressand, K. and Andrieux, A. (2010) Chronic administration of atypical antipsychotics improves behavioral and synaptic defects of STOP null mice. *Psychopharmacology (Berl)*, **208**, 131-141.
- 55 Andrieux, A., Salin, P.A., Vernet, M., Kujala, P., Baratier, J., Gory-Faure, S., Bosc, C., Pointu, H., Proietto, D., Schweitzer, A. *et al.* (2002) The suppression of brain cold-stable microtubules in mice induces synaptic defects associated with neuroleptic-sensitive behavioral disorders. *Genes Dev*, **16**, 2350-2364.

## Figures titles and legends

### Figure 1. Pedigrees and brain imaging results for the three families described in this study.

(a) Pedigree for family 1 with key indicating the genetic data generated in this study. *SVBP* status is indicated under analysed individuals. (b) Pedigree for family 2. (c) Pedigree for family 3. (d) MRI images for individual II-3 from family 2 taken at age 6 years 3 months – sagittal T1-weighted (left) and axial T2-weighted images through the level of the basal ganglia (middle) and corona radiata (right) show a generally thin but fully formed corpus callosum and reduced bulk of the periventricular white matter with enlargement and scalloping of the ventricular outlines. There is no gliotic damage to the white

matter, myelination is appropriate and the basal ganglia/cortex appear normal. (e) MRI images as in (d) for individual II-3 from family 3 at age 3 years 5 months. Similar findings are observed, with a thin corpus callosum and reduced periventricular white matter bulk with mildly enlarged/scalloped ventricles. For family 1, MRI analysis identified similar features (images not available).

## **Figure 2. Impact of SVBP deficiency on detyrosination parameters**

(a) Effect of pathogenic SVBPs on detyrosination activity of VASH1. Immunoblots of tubulin detyrosination assays performed in HEK293T cells. Plasmids encoding VASH1-eGFP and wild-type (WT) or mutants SVBP-myc-Flag were cotransfected into cells. Q28 and K13 respectively correspond to p.Q28\* and p.K13Nfs\*18, with myc-Flag epitopes added at their C-terminus. Antibodies specific to detyrosinated tubulin are used to assess detyrosinase activity. Antibodies against GAPDH, eGFP (VASH1) or Flag (SVBP) reveal the amounts of protein in the extract. Non-transfected cells reveal the endogenous levels of detyrosinated tubulin. (+) refers to wild-type VASH1 or SVBP. (b-e) Comparison of  $\alpha$ -tubulin modifications in wild-type and *Svbp* KO brain extracts. (b) Representative immunoblots obtained with brain protein extracts from 3 wild-type and 3 *Svbp* KO mice. Specific antibodies were used to detect tyrosinated, detyrosinated and  $\Delta 2$   $\alpha$ -tubulin pools. GAPDH staining is representative of the amount of proteins in the extract. (c-e) Quantification of results obtained as in (b). Triplicate immunoblots of the 6 protein extracts were analysed. Quantity in *Svbp* KO is expressed as percentage of quantity in wild-type (after correction using GAPDH signal) for (a) tyrosinated tubulin level, (b) detyrosinated tubulin level, and (c)  $\Delta 2$  tubulin levels. Student *t* test two tails, \*\*\*  $p < 0.001$ , \*\*\*\*  $p < 0.0001$ .

**Figure 3. Effect of SVBP deficiency on neurite outgrowth and axonal differentiation.** Hippocampal neurons were cultured from E17.5 wild type or *Svbp* KO mice brain embryos. (a-e) After 2 days of differentiation in vitro (2 DIV), neurons were fixed and immunolabeled. (a) Tyrosinated and detyrosinated  $\alpha$ -tubulin levels were imaged using the same antibodies as in immunoblots. (b-e) 20 neurons per embryo, from 6 different wild-type or *Svbp* KO embryos were analyzed using NeuronJ plugging from ImageJ software on immunofluorescence images (generated as in a). (b) Proportion of

stage III neurons (bearing an axon, an index of neuronal differentiation) is represented as mean  $\pm$  SEM (n = number of analyzed embryos). **(c-e)** Morphometric analyses of 2 DIV neurons including axonal length **(c)** and branching parameters **(d,e)** are represented as means  $\pm$  SEM (n = number of analyzed neurons). Mann-Whitney test, \*\*  $p < 0.01$  and \*  $p < 0.05$ . **(f)** Sholl analysis of dendritic arborization of WT and *Svbp* KO neurons cultured 17 DIV. The graph shows the mean number of dendritic branches as a function of radial distance (n=60 neurons per condition, 10 to 20 neurons per embryo, 4 WT and 3 *Svbp* KO embryos). Statistics calculated by Two-Way ANOVA followed by Sidak's Multiple Comparisons test. Error bars indicate SEM. \*  $p < 0.05$ , \*\*  $p < 0.01$ , \*\*\*  $p < 0.001$ , \*\*\*\*  $p < 0.0001$ .

#### **Figure 4. *Svbp* deletion induce brain morphological defects**

**(a)** Representative 3D reconstructions of wild-type brain areas built from high spatial resolution MRI- $T_{1w}$  data. Each brain structure is represented with a specific color: cerebellum (CB, pink); cortex (CX, yellow); olfactory bulbs (OB, green); brainstem (BS, light yellow); hippocampal formation (HF, dark green); corpus callosum (cc, dark purple); caudate putamen (CPU, dark blue); colliculi (CO, red); thalamus (TH, magenta); fimbria (fi, light green); hypothalamus (HP, khaki); globus pallidus (GP, light blue) and anterior commissure (ac, light pink). **(b)** Quantification of the volumes of the different cerebral regions represented in panel A. The dot plots show volumes for these regions (in  $\text{mm}^3$ ) of wild-type and KO mice. Percent volume reduction in SVBP-KO mice is indicated in red. Black bars represent the mean (n = 8 for wild-type and *Svbp* KO mice, Student *t* test two tails, \*  $p < 0.05$ ; \*\*  $p < 0.01$ ; \*\*\*  $p < 0.001$ ).

#### **Figure 5. *Svbp* KO mice exhibit behavioural defects**

Wild-type (WT) and *Svbp* KO mice were compared for **(a)** the travelled distance in the open field, **(b)** the time spent in social exploration time by the resident after either 1 or 3 weeks of isolation. n = 9 and 11, respectively for WT and KO, and **(c)** the number of buried marbles at the end of the marbles burying test. **(d)** Average time spent in each house by each group of mice (n = 7 for WT and KO) during the 10 days of training in the Hamlet. Horizontal bars represent means, Mann-Whitney test, two tails: \*  $p < 0.05$ ; \*\*  $p < 0.01$ .

909

910 **Abbreviations**

911 Days of differentiation in vitro (DIV)

912 Knockout (KO)

913 Loss of Function (LoF)

914 Magnetic resonance imaging (MRI)

915 Multiplicity of infection (MOI)

916 Whole genome sequencing (WGS)

917 Wildtype (WT)

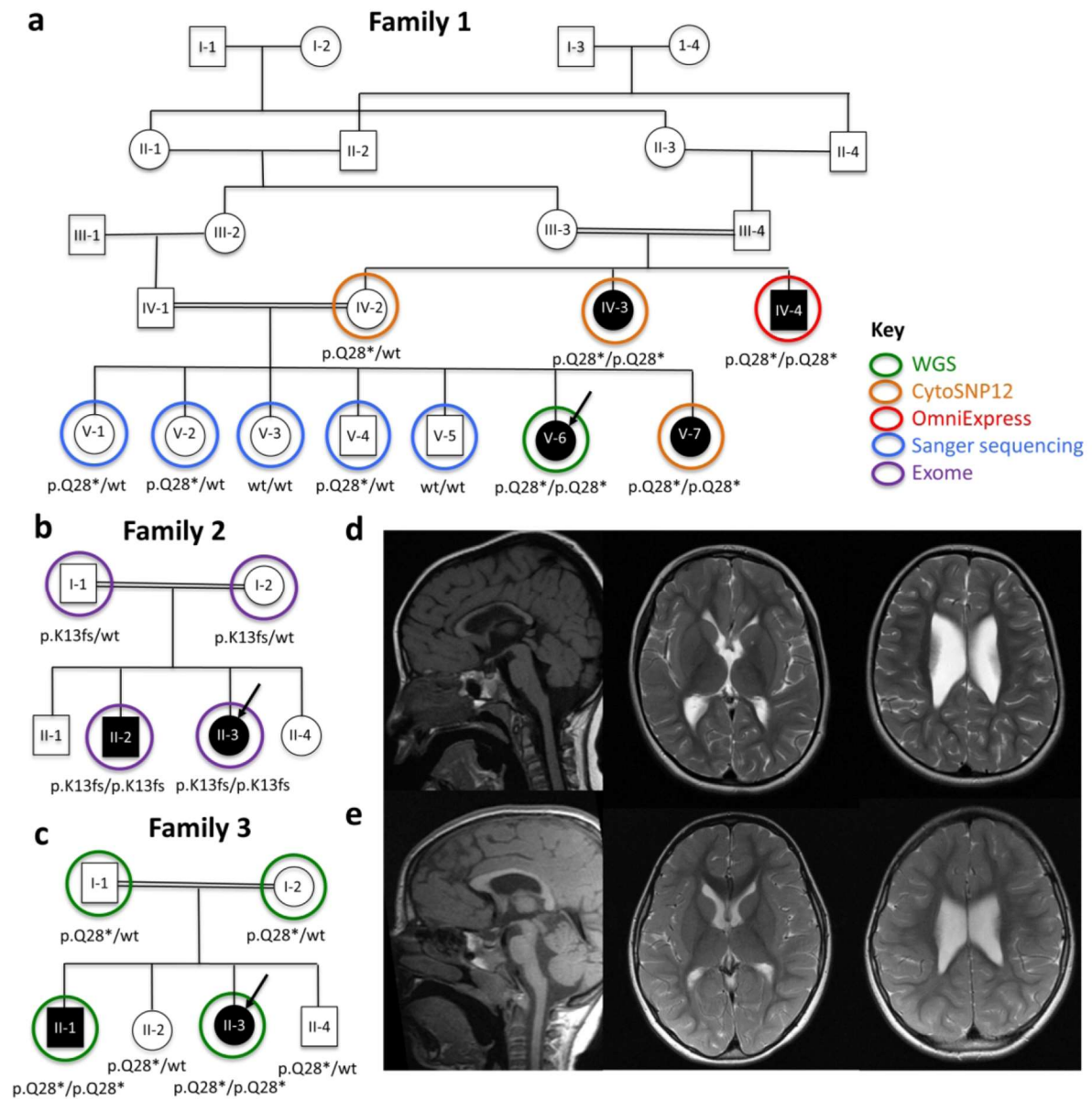
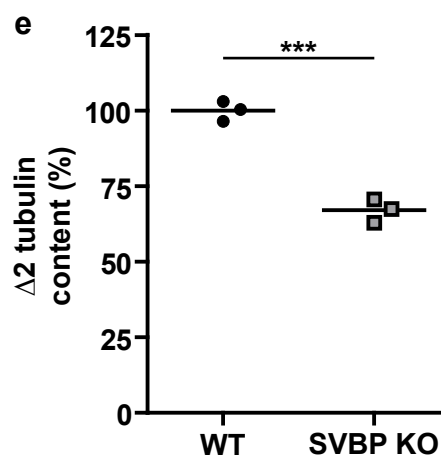
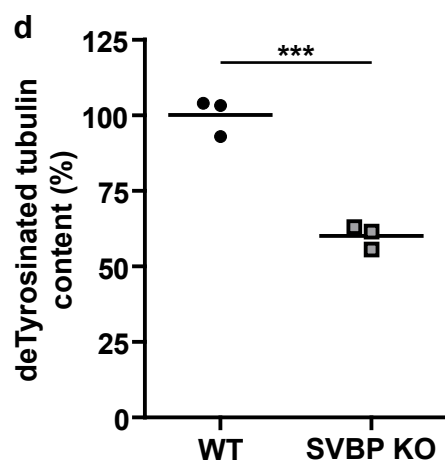
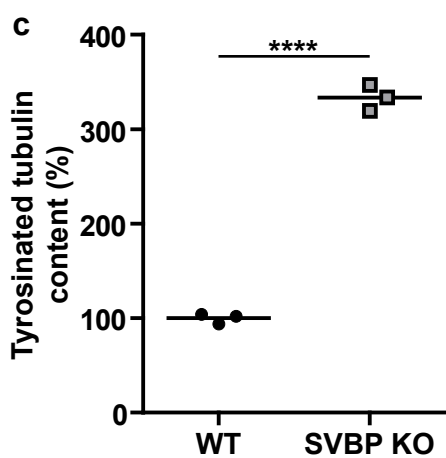
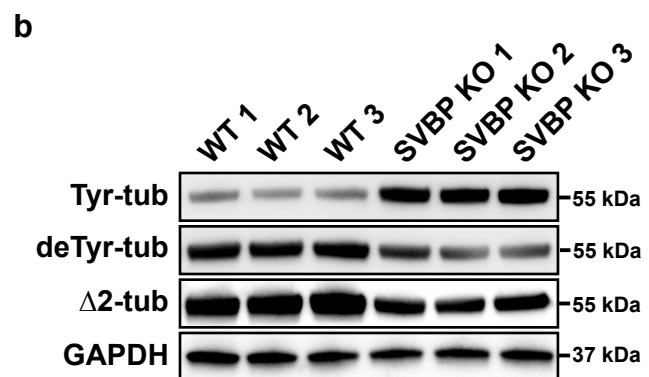
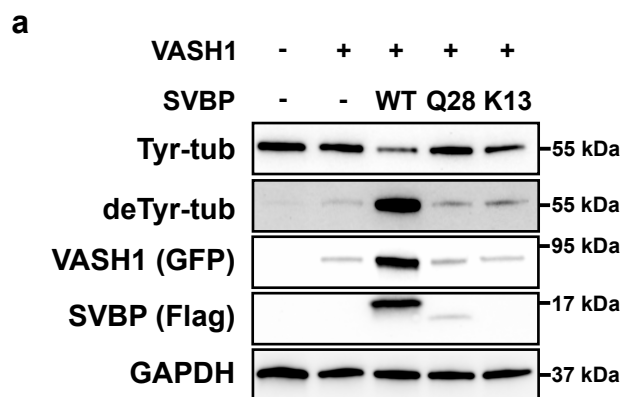
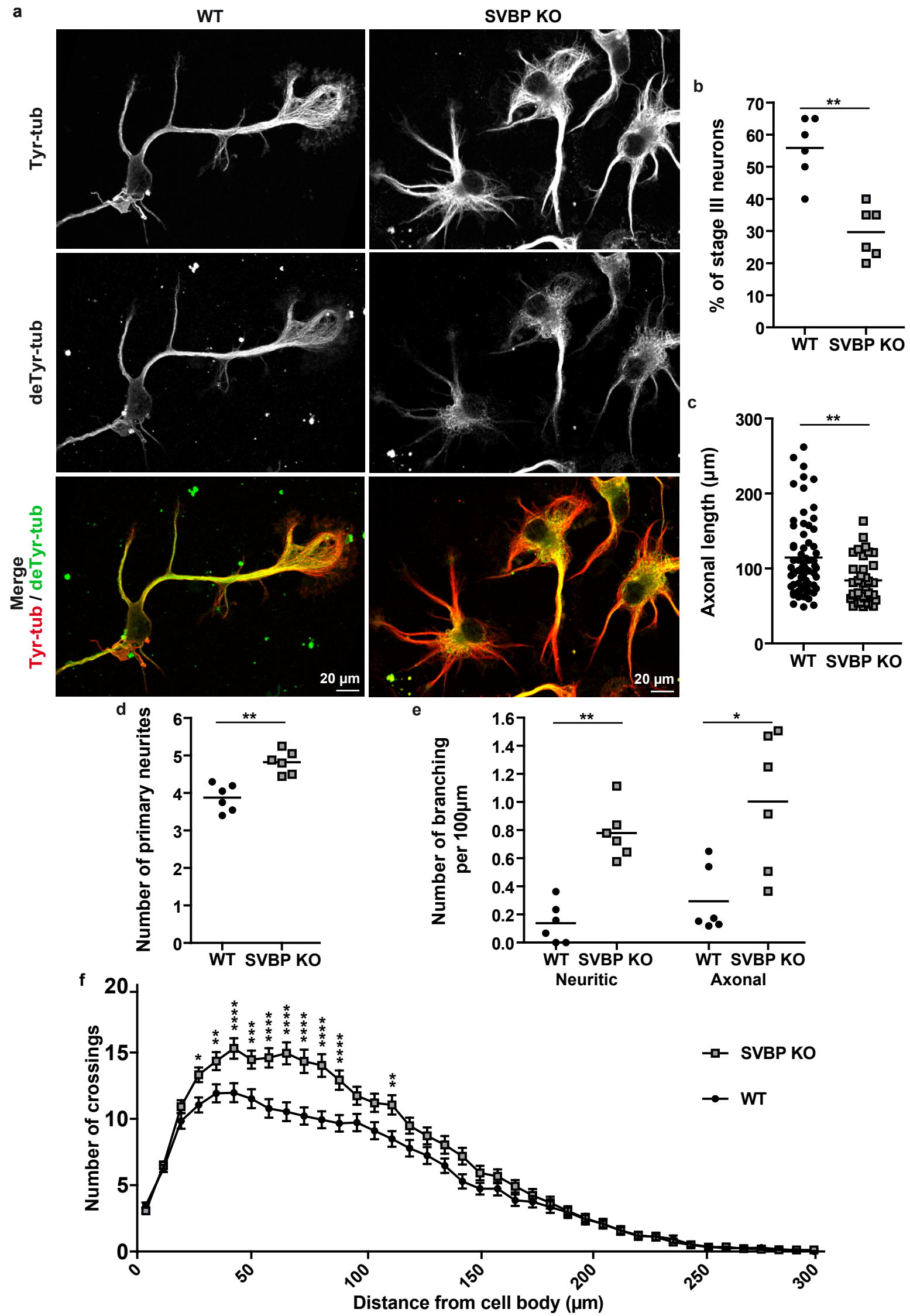
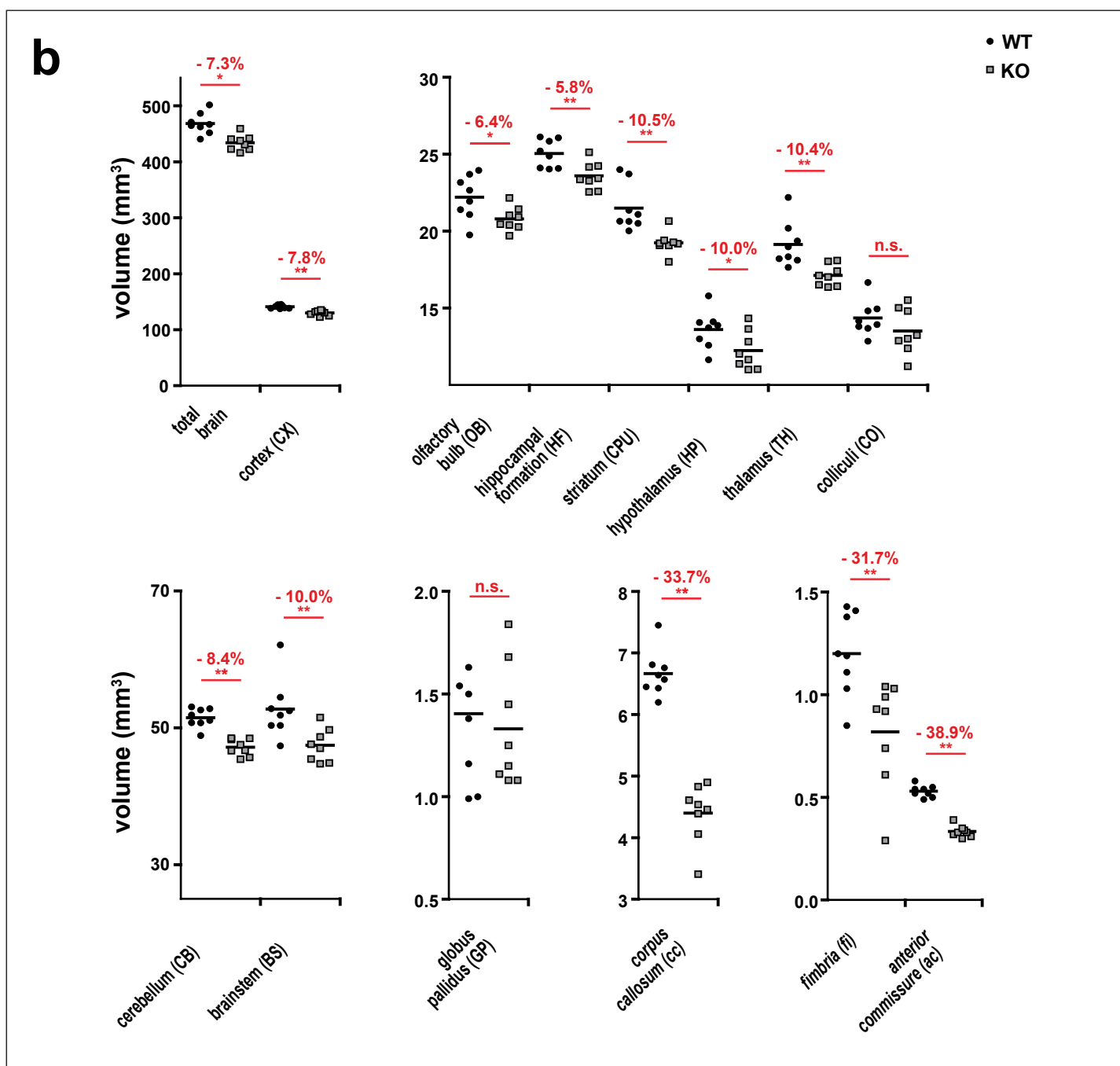
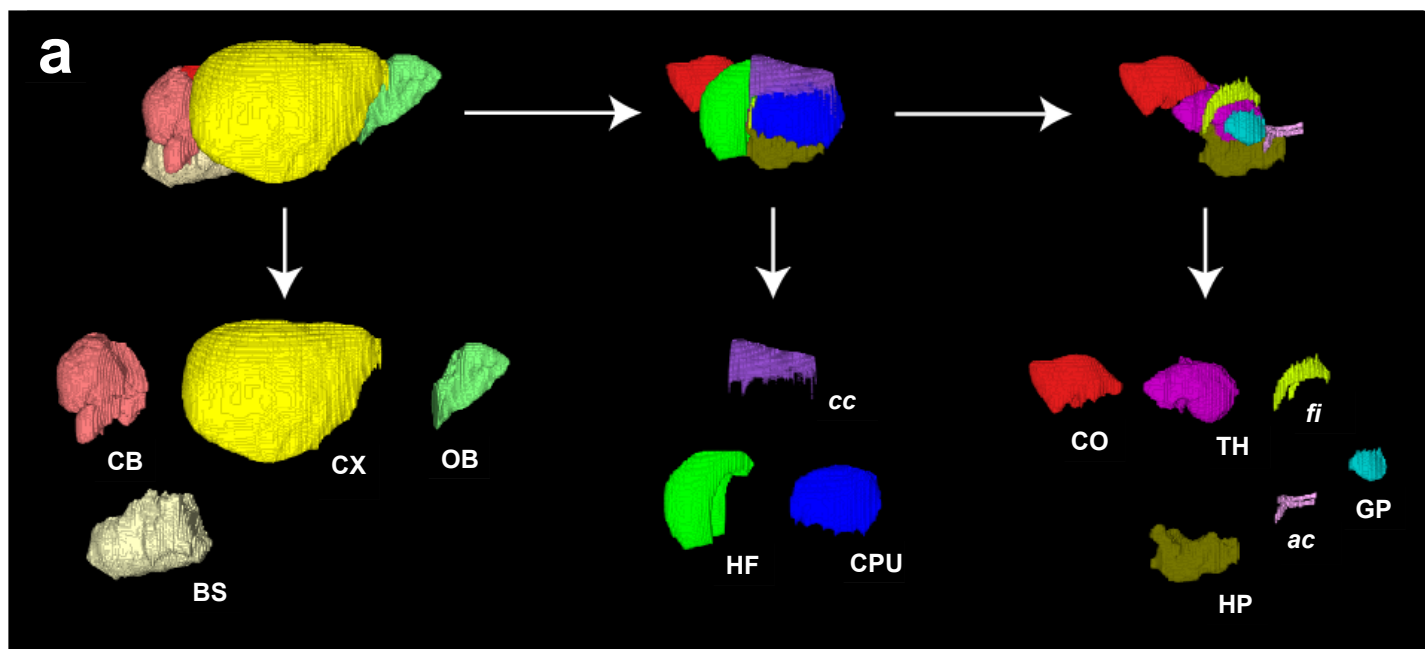
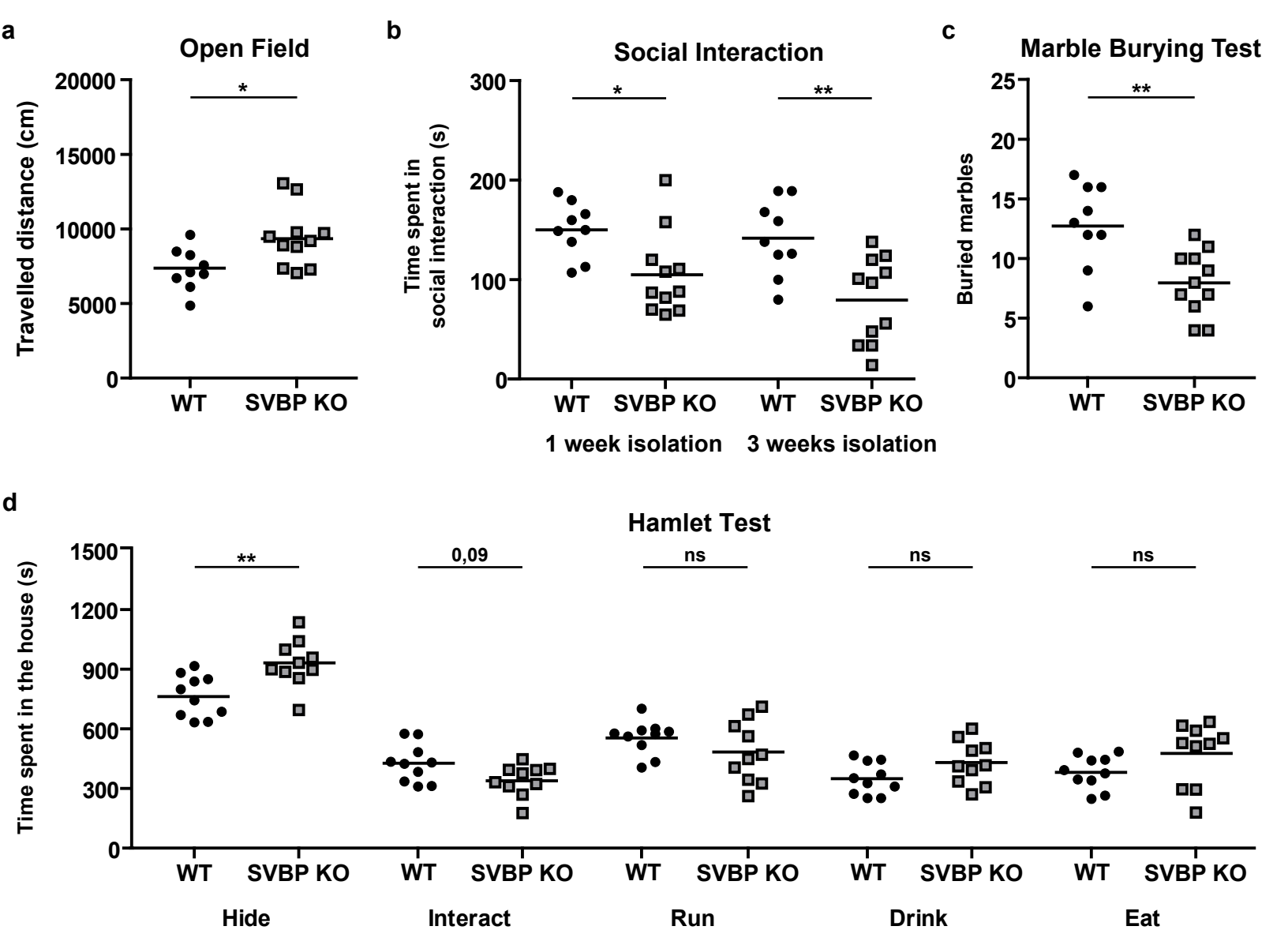


Fig 1: Pedigrees and brain imaging results for the three families described in this study









## Supplemental Methods

### Search for other candidate pathogenic variants in WGS data from Family 1

In addition to the simple recessive model, we also considered a compound heterozygous model in the three regions that were IBD2 between all affected individuals but not homozygous (totalling 10 Mb), but no good candidates were found.

Additionally, several methods were used to search for copy number variants (CNVs), as described.<sup>1</sup> These included a) generating count profiles in 10 kb bins along the genome and correcting for noise due to biases in sequence composition, b) OncoSNP-SEQ<sup>2</sup> and c) ExomeDepth.<sup>3</sup> In addition to these, GenomeSTRiP<sup>4</sup> was used to search for intermediate-sized deletions (50-50,000 bp) that would have been missed by arrayCGH and Platypus.<sup>5</sup> We filtered the calls based on their frequency in other WGS500 samples (MAF < 0.5%). We considered the closest gene to each deletion as the affected gene, and, for the compound recessive model, treated large deletions and SNVs/small indels together. We found no rare structural variants within the linkage region.

We also considered noncoding variants with MAF < 0.5%. To narrow the search, we focused on variants that were within conserved blocks of DNA identified using phastCons<sup>6</sup>, and that fell in regulatory regions annotated by the Ensembl Variant Effect Predictor<sup>7</sup>, which were identified using information about various chromatin marks and transcription factor binding sites. This did not reveal any variants that seemed more likely to be causal than the p.(Q28\*) variant in *SVBP*.

To allow for the possibility of a pedigree error, we analyzed the WGS data from individual V-6 alone to check that there were no more likely causal variants. We retained only high confidence variants with at least 5x coverage, a call quality of at least 20 and which passed upstream pipeline filtering. We also required for variants to be seen in both +ve and -ve strand reads. In a previous study, analysis of data from the WGS500 project identified regions of the genome where variant genotype calls are typically unreliable and varied based on which analytical pipeline had been used.<sup>8</sup> We therefore excluded variants situated in these regions as well.

We then applied a number of population allele frequency filters, removing variants that were seen at > 0.1% in at least one of the following datasets: the 1000 genomes project (phase3v5b), NHLBI ESP exomes (ESP6500SI-V2), ExAC (v0.3.1; using subpopulation with highest allele frequency), gnomAD (v2.0.1; using subpopulation with highest allele frequency).

We then restricted to coding variants (missense, in-frame indels, frameshifting indels, or stop gain, +/- 2 bp splice site variants and variants predicted to disrupt splicing by MaxEntScan). Lastly, we filtered for variants that were called homozygous and were seen in at least 80% of reads.

### **Sanger sequencing for variant validation and confirmation of segregation**

For Sanger validation of the c.82C>T; p.(Q28\*) variant we PCR amplified a 269 bp DNA fragment with primers 5'-GCTCGCTGTCAGTTCTCCTT-3' and 5'-AAGATCTGCCTCTTTCTGTACCA-3' in 25 µl reaction volumes using the FastStart Taq DNA Polymerase PCR kit (Roche). Amplicons were run on a 1.8% agarose gel for size confirmation and then purified using exonuclease I and shrimp alkaline phosphatase. Sanger sequencing was performed using BigDye chemistry (v3.1).

### **RNA analysis of clinical samples**

2.5 ml of whole blood was collected from all available family members (IV-2, IV-3, IV-4, V-6 and V-7) into PAXgene blood RNA tubes (PreAnalytiX). RNA was extracted using PaxGene blood RNA extraction kit (Qiagen) according to the manufacturer's guidelines. RNA was quantified using the nanodrop ND-1000 and RIN values were obtained using the 2100 Bioanalyser using RNA 6000 Pico chips (Agilent Technologies). RIN values were all 7.7-8.8, indicating good quality RNA. Reverse transcriptase (RT) reactions were performed using 500 ng of heat-denatured RNA as template with the QuantiTect kit (Qiagen) which uses a mix of oligo-dT and random primers. RT-negative reactions were set up in parallel to ensure there was no amplification from any residual genomic DNA.

A 265 bp segment spanning exons 2 and 3 of *SVBP* cDNA was amplified with primers SVBP-2F 5'-AGAAATATCCAGAAGTCAAGCCA-3' and SVBP-3R 5'-TCTCAAAGCTCTCAGGATCCC-3'.

Amplicons were size-checked and then purified as described above. Sanger sequencing was performed using BigDye chemistry (v3.1) and run on an ABI 3730XL machine.

Quantitative PCR was also performed on the same cDNA samples using the SVBP-2F/3R primers and the iQ5 SYBR Green Supermix, using the iQ5 realtime-PCR machine (BIO-RAD). Ct values derived from a 234 bp *ACTB* amplicon were used to normalise expression. Expression was then compared to two control cDNA samples (prepared using the same method) using the  $2^{-\Delta\Delta Ct}$  formula.<sup>9</sup> qPCRs were performed in triplicate and the experiment was performed three times.

### **Genotyping and backcrosses**

PCR amplifications were performed directly on alkaline lysates of toe clips. Briefly, each toe was incubated 30 min at 95°C in 100 µL of alkaline solution (NaOH 25 mM, EDTA 0.2 mM, pH 12.0). Neutralization was performed by adding 100 µl Tris 40 mM, pH 5.0. Two microliters of lysates were analyzed by PCR (25 µL) with appropriate primers (Table S1) and GreenTaq Mix (Euromedex), according the following protocol: 95°C for 10 min, 33 cycles of [95°C for 30 sec / 58°C for 30 sec / 72°C for 30 sec], 72°C for 10 min. Indels in F0 mice were identified by Sanger sequencing of PCR products (Eurofins). The sequencing Sanger electropherograms obtained from mosaic F0 mice were analyzed using the TIDE software which decomposes sequencing traces and estimates the respective contribution of each PCR fragment.<sup>10</sup> We thus selected a mosaic F0 mouse carrying a 11 nt deletion introducing a frameshift and only four additional chimeric residues. This F0 mouse was further backcrossed with C57BL/6 mice to select the  $\Delta 11$  deletion among the F0 mosaic indels. Tail fragments of the F1 mice and their successive backcrosses were lysed as above. Two microliters of lysates were then analyzed by PCR (25 µL), using forward primers targeting either the wild-type allele or the  $\Delta 11$  deletion junction, a common reverse primer (Table S1) and GreenTaq Mix, according the following protocol: 95°C for 5 min, 33 cycles of [95°C for 30 sec / 50°C for 30 sec / 72°C for 30 sec], 72°C for 2 min. Amplicons were run on a 1.8% agarose gel for presence and size confirmation. PCR with the 5' WT-for primer generates a fragment only with the DNAs of wild-type and heterozygous mice. PCR with the 5'  $\Delta 11$ -for primer generates a fragment only with the DNAs of *Svbp* KO and heterozygous mice.

### **Y-Maze test**

The Y-Maze test was performed as described previously.<sup>11</sup> Spontaneous alternation in a Y-maze is based on the innate tendency of rodents to explore new environments, and the short-term storage and retrieval of relevant information are related to working memory. The apparatus consists of three walled arms (L20 x l8 x h16 cm) radiating at an angle of 120° from each other. Without prior habituation to the apparatus, each mouse was placed into the starting arm and allowed to move freely through the maze during 5 min. A mouse was considered to have entered an arm when all four paws were positioned in the arm runway. An alternation was defined as entries into all 3 arms on consecutive choices. The alternation score (%) for each mouse was calculated as the ratio of the actual number of alternations to the possible number (defined as the total number of arm entries minus 2), as shown by the following equation: % alternation = [(Number of alternations) / (Total arm entries-2)] × 100.

#### **Novelty Suppressed Feeding (NSF) test**

The NSF test was performed as described previously.<sup>12</sup> It is an anxiety-based conflict test where the motivation to eat competes with fear of a brightly lit area. The NSF test was performed for 15 min. Briefly, animals had no access to food in their home cage for 20 h prior to performing the test. For the test, a single food pellet was placed on a brightly-lit white paper platform placed in the center of a plastic box (L37 x l57 x h20 cm) where the floor was covered with approximately 2 cm of bedding. The animal was placed in a corner of the box and the latency to eat was recorded.

#### **Elevated Plus Maze**

This labyrinth consists of two intersecting tracks, placed at 60 cm from the ground. One track had no walls (two open arms), while the other had dark walls 15 cm high (two arms closed). Each arms measure L30 cm x l7 cm. The mice were placed in the center of the labyrinth, facing an open arm, and allowed to explore for 5 min. A camera placed above the labyrinth recorded the movements of the animal and the tests were analyzed using the Ethovision XT14 software (Noldus, Wageningen, Netherlands). Total distance travelled, number of entries and time spent in each arm were monitored.

## **Extended authors**

### **WGS500 Consortium membership: names and affiliations of authors**

Steering Committee: Peter Donnelly (Chair)<sup>1</sup>, John Bell<sup>2</sup>, David Bentley<sup>3</sup>, Gil McVean<sup>1</sup>, Peter Ratcliffe<sup>1</sup>, Jenny C. Taylor<sup>1,4</sup>, Andrew Wilkie<sup>4,5</sup>

Operations Committee: Peter Donnelly (Chair)<sup>1</sup>, John Broxholme<sup>1</sup>, David Buck<sup>1</sup>, Jean-Baptiste Cazier<sup>1</sup>, Richard Cornall<sup>1</sup>, Lorna Gregory<sup>1</sup>, Julian Knight<sup>1</sup>, Gerton Lunter<sup>1</sup>, Gil McVean<sup>1</sup>, Jenny C. Taylor<sup>1,4</sup>, Ian Tomlinson<sup>1,4</sup>, Andrew Wilkie<sup>4,5</sup>

Sequencing & Experimental Follow up: David Buck (Lead)<sup>1</sup>, Christopher Allan<sup>1</sup>, Moustafa Attar<sup>1</sup>, Angie Green<sup>1</sup>, Lorna Gregory<sup>1</sup>, Sean Humphray<sup>3</sup>, Zoya Kingsbury<sup>3</sup>, Sarah Lambie<sup>1</sup>, Lorne Lonie<sup>1</sup>, Alistair T. Pagnamenta<sup>1</sup>, Paolo Piazza<sup>1</sup>, Guadelupe Polanco<sup>1</sup>, Amy Trebes<sup>1</sup>

Data Analysis: Gil McVean<sup>1</sup> (Lead), Peter Donnelly<sup>1</sup>, Jean-Baptiste Cazier<sup>1</sup>, John Broxholme<sup>1</sup>, Richard Copley<sup>1</sup>, Simon Fiddy<sup>1</sup>, Russell Grocock<sup>3</sup>, Edouard Hatton<sup>1</sup>, Chris Holmes<sup>1</sup>, Linda Hughes<sup>1</sup>, Peter Humburg<sup>1</sup>, Alexander Kanapin<sup>1</sup>, Stefano Lise<sup>1</sup>, Gerton Lunter<sup>1</sup>, Hilary C. Martin<sup>1</sup>, Lisa Murray<sup>3</sup>, Davis McCarthy<sup>1</sup>, Andy Rimmer<sup>1</sup>, Natasha Sahgal<sup>1</sup>, Ben Wright<sup>1</sup>, Chris Yau<sup>6</sup>

<sup>1</sup>The Wellcome Centre for Human Genetics, Roosevelt Drive, Oxford, OX3 7BN, UK

<sup>2</sup>Office of the Regius Professor of Medicine, Richard Doll Building, Roosevelt Drive, Oxford, OX3 7LF, UK

<sup>3</sup>Illumina Cambridge Ltd., Chesterford Research Park, Little Chesterford, Essex, CB10 1XL, UK

<sup>4</sup>NIHR Oxford Biomedical Research Centre, Oxford, UK

<sup>5</sup>Weatherall Institute of Molecular Medicine, John Radcliffe Hospital, Headington, Oxford OX3 9DS, UK

<sup>6</sup>Imperial College London, South Kensington Campus, London, SW7 2AZ, UK

### **Genomics England Research Consortium: names and affiliations of authors**

John C. Ambrose<sup>1</sup>, Emma L. Baple<sup>1</sup>, Marta Bleda<sup>1</sup>, Freya Boardman-Pretty<sup>1,2</sup>, Jeanne M. Boissiere<sup>1</sup>, Christopher R. Boustred<sup>1</sup>, Mark J. Caulfield<sup>1,2</sup>, Georgia C. Chan<sup>1</sup>, Clare E. H. Craig<sup>1</sup>, Louise C. Daugherty<sup>1</sup>, Anna de Burca<sup>1</sup>, Andrew Devereau<sup>1</sup>, Greg Elgar<sup>1,2</sup>, Rebecca E. Foulger<sup>1</sup>, Tom Fowler<sup>1</sup>, Pedro Furió-Tarí<sup>1</sup>, Joanne M. Hackett<sup>1</sup>, Dina Halai<sup>1</sup>, James E. Holman<sup>1</sup>, Tim J. P. Hubbard<sup>1</sup>, Rob Jackson<sup>1</sup>, Dalia Kasperaviciute<sup>1,2</sup>, Melis Kayikci<sup>1</sup>, Lea Lahnstein<sup>1</sup>, Kay Lawson<sup>1</sup>, Sarah E. A. Leigh<sup>1</sup>, Ivonne U. S. Leong<sup>1</sup>, Javier F. Lopez<sup>1</sup>, Fiona Maleady-Crowe<sup>1</sup>, Joanne Mason<sup>1</sup>,

Ellen M. McDonagh<sup>1,2</sup>, Loukas Moutsianas<sup>1,2</sup>, Michael Mueller<sup>1,2</sup>, Nirupa Murugaesu<sup>1</sup>, Anna C. Need<sup>1,2</sup>, Chris A. Odhams<sup>1</sup>, Christine Patch<sup>1,2</sup>, Daniel Perez-Gil<sup>1</sup>, Dimitris Polychronopoulos<sup>1</sup>, John Pullinger<sup>1</sup>, Tahrima Rahim<sup>1</sup>, Augusto Rendon<sup>1</sup>, Pablo Riesgo-Ferreiro<sup>1</sup>, Tim Rogers<sup>1</sup>, Mina Ryten<sup>1</sup>, Kevin Savage<sup>1</sup>, Kushmita Sawant<sup>1</sup>, Richard H. Scott<sup>1</sup>, Afshan Siddiq<sup>1</sup>, Alexander Sieghart<sup>1</sup>, Damian Smedley<sup>1,2</sup>, Katherine R. Smith<sup>1,2</sup>, Alona Sosinsky<sup>1,2</sup>, William Spooner<sup>1</sup>, Helen E. Stevens<sup>1</sup>, Alexander Stuckey<sup>1</sup>, Razvan Sultana<sup>1</sup>, Ellen R. A. Thomas<sup>1,2</sup>, Simon R. Thompson<sup>1</sup>, Carolyn Tregidgo<sup>1</sup>, Arianna Tucci<sup>1,2</sup>, Emma Walsh<sup>1</sup>, Sarah A. Watters<sup>1</sup>, Matthew J. Welland<sup>1</sup>, Eleanor Williams<sup>1</sup>, Katarzyna Witkowska<sup>1,2</sup>, Suzanne M. Wood<sup>1,2</sup>, Magdalena Zarowiecki<sup>1</sup>

<sup>1</sup>Genomics England, London, UK

<sup>2</sup>William Harvey Research Institute, Queen Mary University of London, London, EC1M 6BQ, UK.

#### **Author contributions statement**

HCM analyzed the genetic data for family 1 and together with JCT, EB and MJM jointly directed the project. ATP performed co-segregation testing, RNA analysis and reviewed genomic data for families 2 and 3. EMB, AAE, CD, SJ, SM, IW, PB and LL helped provide and review clinical data. AS performed neuroradiological assessment of human subjects. CB, AA and MJM oversaw the mice generation project. CB assisted by ED developed the CRISPR/Cas9 and genotyping strategies, and engineered plasmids constructs. FV assisted for plasmids amplifications and mice genotyping. PH and FV analyzed the effect of pathogenic SVBPs on deetyrosination and tubulin modifications levels in cells and tissues supervised by MJM. JCD provided expertise on mice brain imaging and morphometry, and prepared brains for MRI. ELB supervised preclinical anatomical MRI performed by IU. PH performed morphometric analysis, and ED images processing and statistical analysis. PH and SC performed mice behavior experiments supervised by SG, TM and AA. LP performed the neuron experiments and analyzed the data with the help of PH. HCM, MJM, AA and ATP wrote the manuscript with the contribution of all co-authors.

## Supplementary Figures and Tables

Supplemental data include six figures and two tables

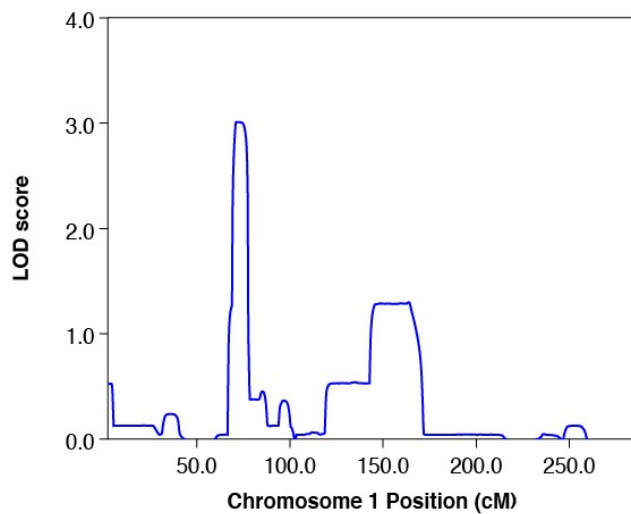


**Figure S1. Results from linkage analysis in Family 1.** We show the LOD scores on chr1 only since this was the only chromosome containing a significant linkage peak.

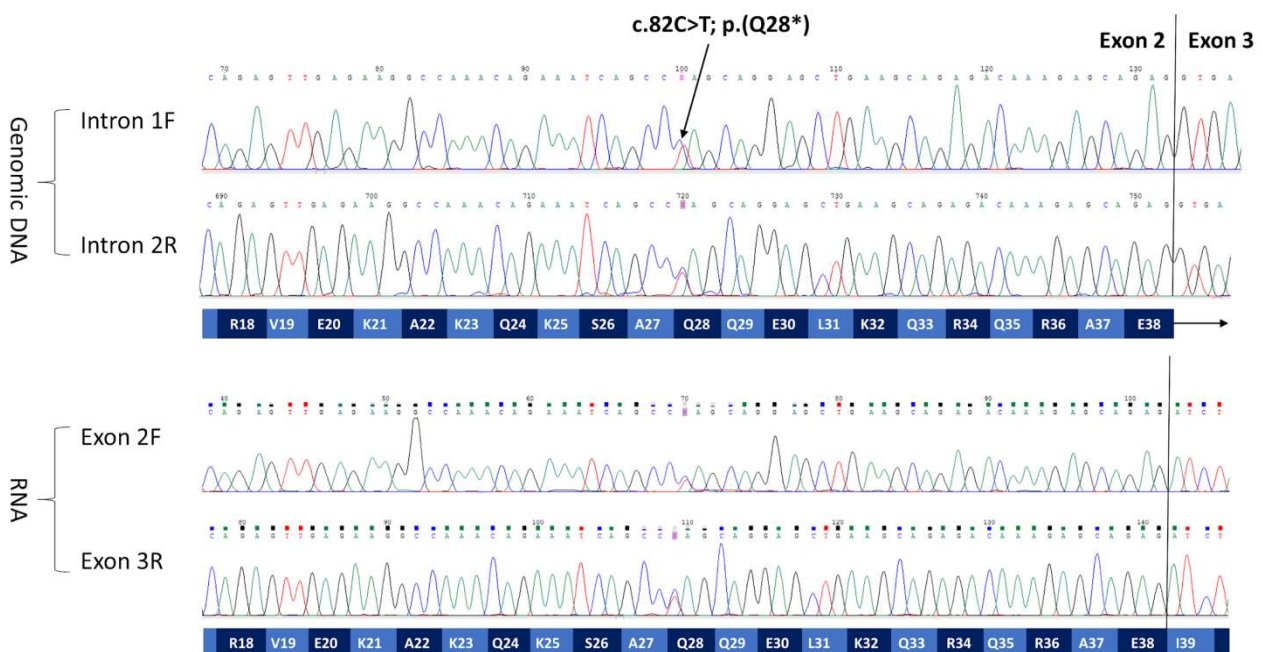


**Figure S2. Bidirectional Sanger sequencing of genomic DNA and RNA for heterozygous individual IV-2.** For ease of comparison, electropherograms from RNA are shown directly below the trace obtained using the genomic DNA. The positions of the primers used for sequencing are labelled on the left of the figure. Peaks corresponding to the wild-type and c.82C>T alleles are of similar height, matching what is seen for genomic DNA. This suggests that the mutant RNA is not degraded significantly. Sequencing of RNA from all 4 affected family members (IV-3, IV-4, V-6, V-7; data not shown) further confirmed homozygosity of the variant.

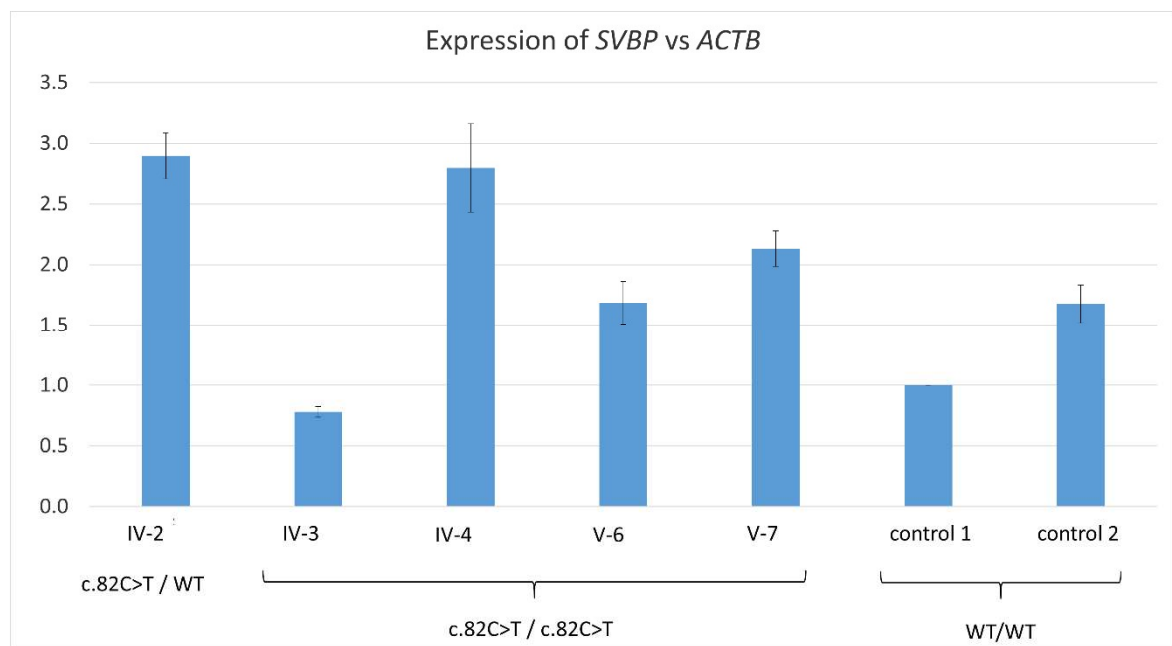


**Figure S3. Quantitative RT-PCR of RNA from individuals IV-2, IV-3, IV-4, V-6 and V-7.** Expression of *SVBP* was normalised with respect to *ACTB*. Relative RNA expression in family member was then compared to the first of two control samples. qPCRs were performed in triplicate and the experiment was then repeated twice. The error bars represent the standard errors observed across the three experiments. These results are consistent with the mutant *SVBP* transcript not being degraded significantly.

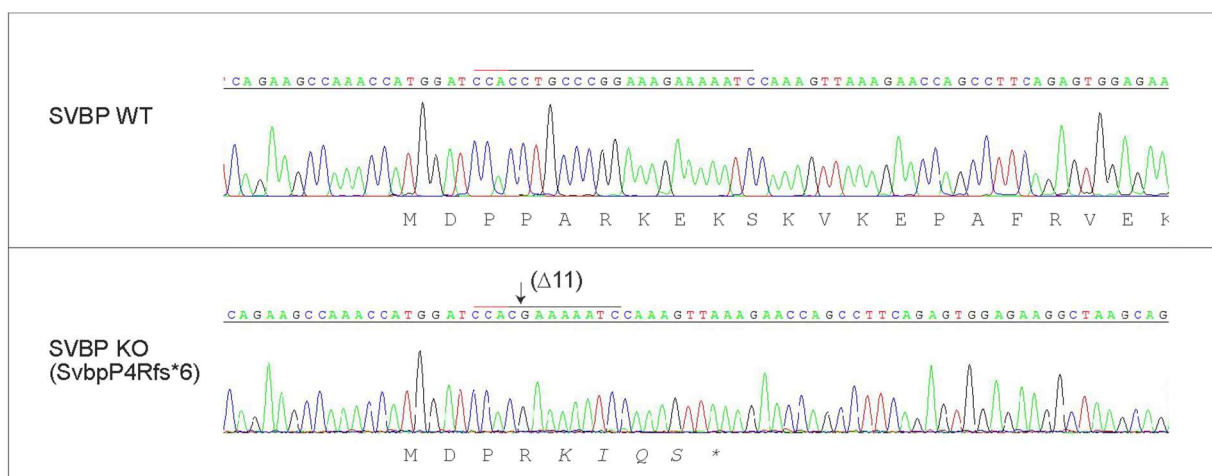


**Figure S4. *Svbp* gene DNA Sanger sequencing of control C57BL/6 mouse (WT) and of knock-out mouse SVBP.** Black and red lines respectively indicate the positions of the crRNA and protospacer adjacent motif (NGG), both located on the complementary strand. Indel site (arrow) and nature of the indel are indicated above the sequence. Translations of SVBP products are shown below the electropherograms, with frameshifted amino-acid in italic.

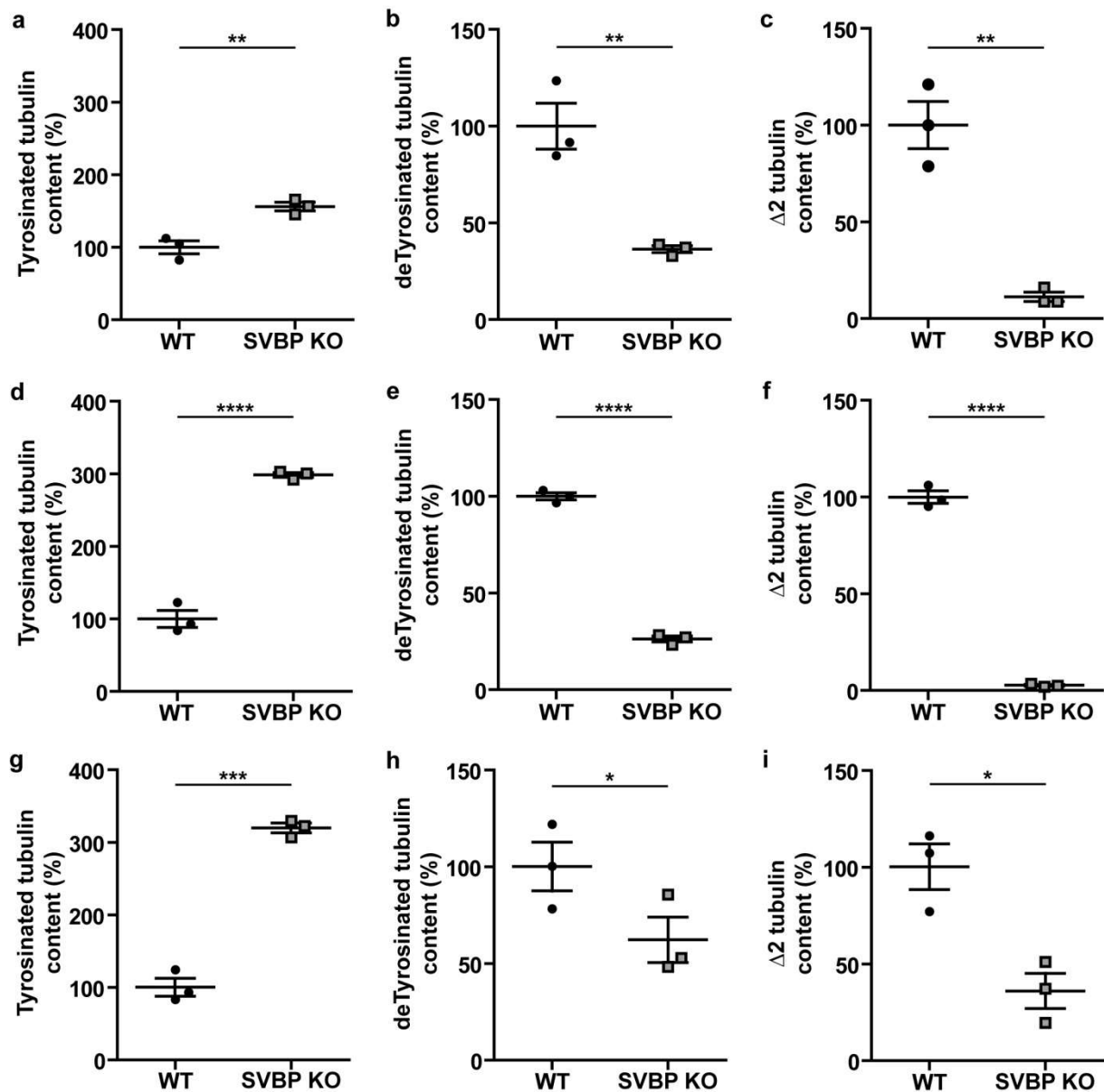


**Figure S5. Comparison of  $\alpha$ -tubulin modifications in wild-type and *Svbp* KO cultured neurons.** Hippocampal neurons were cultured from E17.5 wild type or *Svbp* KO embryos. After 2 (a, b, c), 7 (d, e, f) or 17 days (g, h, i) of differentiation in vitro (2 DIV, 7 DIV or 17 DIV), protein extracts were prepared. Specific antibodies were used to detect tyrosinated, detyrosinated and  $\Delta 2$   $\alpha$ -tubulin pools, and GAPDH staining was used to estimate amount of proteins in the extract. Triplicate immunoblots of the extracts from 3 different cultures were analyzed. Quantity in *Svbp* KO is expressed as percentage of quantity in wild-type (after correction using GAPDH signal) for (a, d, g) tyrosinated tubulin level, (b, e, h) detyrosinated tubulin level, and (c, f, i)  $\Delta 2$  tubulin levels. Student *t* test two tails, \*  $p < 0.05$ , \*\*  $p < 0.01$ , \*\*\*  $p < 0.001$ , \*\*\*\*  $p < 0.0001$ .

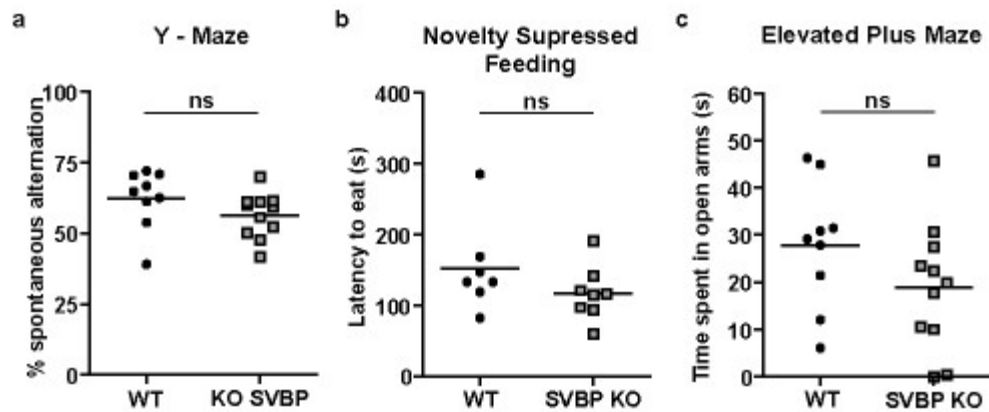


**Figure S6. Behavioral analysis of *Svbp* KO mice.** (a) Percentage of spontaneous alternation in Y-Maze (horizontal bar represents mean, student t-test, two-tails,  $n = 9$  and  $11$  for wild-type (WT) and *Svbp* KO mice respectively,  $p = 0.16$ ). (b) Latency to eat for the novelty suppressed feeding test (horizontal bar represents mean, Mann-Whitney test,  $n = 7$  and  $9$  for WT and *Svbp* KO mice respectively,  $p = 0.11$ ). (c) Time spent in open arms in the elevated plus maze test (the horizontal bar represents the average, Mann-Whitney test,  $n = 9$  and  $11$  for WT and *Svbp* KO mice respectively,  $p = 0.19$ ). ns, not significant.

**Table S1: Phenotypes of affected individuals in families described in this study.**

See separate excel file.

Name	Sequence	PCR size (bp)
tracrRNA	5' AAACAGCAUAGCAAGUUAUAAAGGCUAGUCCGUUAUCAACUUGAAAA AGUGGCACCGAGUCGGUGC [U*U*U*] U3'	
SVBP-crRNA	5' [G*A*U*] UUUUCUUUCCGGGCAGGGUUUUAGAGCUAUGCUGUUUUUG3'	
SVBP-for (F0)	5' CCAGCTTGGGATTCTGACAC3'	591
SVBP-rev (F0)	5' TTCTCGGGCCTTCTCATCTG3'	
WT-for	5' GATCCACCTGCCCCGAAA3'	170
WT-rev/ $\Delta 11$ -rev	5' TTTCTTCCAGCACCCCTCTCC3'	
$\Delta 11$ -for	5' CAAACCATGGATCCACGAAA3'	168
WT-rev/ $\Delta 11$ -rev	5' TTTCTTCCAGCACCCCTCTCC3'	

**Table S2: Description of oligonucleotide used for generation and genotyping of mice.** Note: \* are for phosphothiorate and [ ] for 2'-O-methyl chemical modifications.

## Supplemental References

1. Taylor, J.C., Martin, H.C., Lise, S., Broxholme, J., Cazier, J.B., Rimmer, A., Kanapin, A., Lunter, G., Fiddy, S., Allan, C., et al. (2015). Factors influencing success of clinical genome sequencing across a broad spectrum of disorders. *Nat Genet* 47, 717-726.
2. Yau, C. (2013). OncoSNP-SEQ: a statistical approach for the identification of somatic copy number alterations from next-generation sequencing of cancer genomes. *Bioinformatics* 29, 2482-2484.
3. Plagnol, V., Curtis, J., Epstein, M., Mok, K.Y., Stebbings, E., Grigoriadou, S., Wood, N.W., Hambleton, S., Burns, S.O., Thrasher, A.J., et al. (2012). A robust model for read count data in exome sequencing experiments and implications for copy number variant calling. *Bioinformatics* 28, 2747-2754.
4. Handsaker, R.E., Korn, J.M., Nemesh, J., and McCarroll, S.A. (2011). Discovery and genotyping of genome structural polymorphism by sequencing on a population scale. *Nat Genet* 43, 269-276.
5. Rimmer, A., Phan, H., Mathieson, I., Iqbal, Z., Twigg, S.R.F., Consortium, W.G.S., Wilkie, A.O.M., McVean, G., and Lunter, G. (2014). Integrating mapping-, assembly- and haplotype-based approaches for calling variants in clinical sequencing applications. *Nat Genet* 46, 912-918.
6. Siepel, A., Bejerano, G., Pedersen, J.S., Hinrichs, A.S., Hou, M., Rosenbloom, K., Clawson, H., Spieth, J., Hillier, L.W., Richards, S., et al. (2005). Evolutionarily conserved elements in vertebrate, insect, worm, and yeast genomes. *Genome Res* 15, 1034-1050.
7. McLaren, W., Gil, L., Hunt, S.E., Riat, H.S., Ritchie, G.R., Thormann, A., Flicek, P., and Cunningham, F. (2016). The Ensembl Variant Effect Predictor. *Genome Biol* 17, 122.
8. Popitsch, N., Consortium, W.G.S., Schuh, A., and Taylor, J.C. (2017). ReliableGenome: annotation of genomic regions with high/low variant calling concordance. *Bioinformatics* 33, 155-160.
9. Pfaffl, M.W. (2001). A new mathematical model for relative quantification in real-time RT-PCR. *Nucleic Acids Res* 29, e45.
10. Brinkman, E.K., Chen, T., Amendola, M., and van Steensel, B. (2014). Easy quantitative assessment of genome editing by sequence trace decomposition. *Nucleic Acids Res* 42, e168.
11. Volle, J., Brocard, J., Saoud, M., Gory-Faure, S., Brunelin, J., Andrieux, A., and Suaud-Chagny, M.F. (2013). Reduced expression of STOP/MAP6 in mice leads to cognitive deficits. *Schizophr Bull* 39, 969-978.
12. Jonckheere, J., Deloulme, J.C., Dall'igna, G., Chauliac, N., Pelluet, A., Nguon, A.S., Lentini, C., Brocard, J., Denarier, E., Brugiere, S., et al. (2018). Short- and long-term efficacy of electroconvulsive stimulation in animal models of depression: The essential role of neuronal survival. *Brain Stimul* 11, 1336-1347.

**Table S1:** Phenotypes of affected individuals in families described in this study. -, not known or missing data. AED, Anti epilepsy drugs. Reported centiles are calculated based on growth charts available at [www.rcpch.ac.uk/resources/uk-who-growth-charts-2-18-years](http://www.rcpch.ac.uk/resources/uk-who-growth-charts-2-18-years) and Freeman *et al* 1995 (PMID: 7639543).

	Family 1				Family 2		Family 3		Summary of patients from Iqbal <i>et al</i> 2019 (N=4)
	V-6 (proband)	V-7	IV-3	IV-4	II-2	II-3 (proband)	II-1	II-3 (proband)	
SVBP variant (NM_199342.3) and ClinVar accession ID	c.82C>T; p.Q28* (SCV000926436)				c.39_42del; p.K13Nfs*18 (SCV000926437)		c.82C>T; p.Q28*		All have c.82C>T; p.Q28*
Ethnicity (degree of parental consanguinity)	Pakistani (1st-cousin)				Kuwaiti (1st-cousin once removed)		Pakistani (first-cousin)		Syrian (2nd-cousin) and Pakistani (1st-cousin)
Gender	Female	Female	Female	Male	Male	Female	Male	Female	3 Female, 1 Male
Intellectual disability	Yes (moderate to severe)	Yes (severe)	Yes (moderate to severe)	Yes (moderate to severe)	Yes	Yes	Yes	Yes (severe)	4/4 (moderate to severe)
Speech	Little expressive language, better receptive language (few single words)	Little expressive language (few single words)	Few words	Little expressive language (few words - 3 word sentences)	Few words	Only a few words aged 6	Only 10 words aged 21 years	Delayed speech and language development	3 with delayed speech (1 too young for assessment)
Behavioural problem	Quiet	Loses temper, bangs head, cries, screams	-	-	-	-	-	Autistic behaviour	2 reported to be aggressive
Height	106.9 cm aged 4 years 10 months (50th centile), 122.1 cm aged 7 years 7 months (25th centile)	90.7 cm aged 3 years 4 months (2nd-9th centile), 131.2 cm aged 9 years and 10 months (9th-25th centile)	141.3 cm aged 45 years (<0.4th centile)	158.4 cm aged 39 years (0.4th centile)	-	79 cm aged 2 years (2nd centile)	Unable to stand-flexion deformity at hips and knees	96 cm age 3 years 6 months (25th centile)	<2 SD and -3.62 to -3.90 SD
Head circumference	48.5 cm aged 5 years 4 months (0.4th centile)	45.2 cm aged 3 years and 11 months (<0.4th centile)	56.0 cm aged 45 years (50th-75th centile)	55.5 cm aged 39 years (9th-25th centile)	49.7 cm aged 7 years and 10 months (0.4th centile)	44.5 cm aged 2 years (<0.4th centile); 47.5 cm at 6 years 6 months (<0.4th centile)	46 cm aged 3 years (<0.4th centile)	45 cm (<0.4th centile)	-2.63 to -6.43 SD
Spasticity	Yes (lower limb spasticity with brisk tendon reflexes)	Yes (increased tone in the lower limbs, with pathologically brisk reflexes and extensor plantar responses)	No (walks only with the use of a walking frame, but lower limb tone and reflexes are normal)	Yes (spastic paraparesis with brisk lower limb reflexes and extensor plantar responses; several operations to release contractures at his hips and ankles)	Yes (generalized hypertonia predominantly in both lower limbs, easily elicited reflexes, unsteady spastic gait)	Yes (generalized hypertonia predominantly in both lower limbs, ankle clonus, easily elicited reflexes, unsteady spastic gait and toe walking)	Yes (spastic diplegia and non-ambulant)	Yes (progressive spasticity with delayed gross and fine motor development)	No (4/4 with muscular hypotonia)
Gross motor development	Delayed (walked at > 24 months)	Delayed (walked at 24 months)	Delayed (walked at 7 years)	Delayed (walked at 5 years)	-	-	'Walks on knees'	Moderately delayed (walked at 14 months). Needs splints	Delayed (walked at 2-3 years)
Brain imaging results	MRI showed irregular ventricular margins and a thin corpus callosum (data not shown)	MRI showed dysgenic corpus callosum with dysmorphic ventricles; slight prominence of CSF spaces; normal cisterna magna, white matter, deep grey structures and calcification (data not shown)	MRI not available	MRI not available	-	MRI showed a thin corpus callosum, dilated ventricles with poor volume of white matter (Fig. 1d)	-	MRI detected a thin corpus callosum and reduced periventricular white matter bulk with mildly enlarged ventricles (Fig. 1e)	CT scan performed for 2/4 and normal brain structures reported (data not shown)
Seizures	-	Single episode of status epilepticus as a 2 year old; ongoing seizure disorder controlled by AEDs (resolved as teenager)	Seizures as teenager aged 13-14 years	Seizures as an infant. seizures when young, resolved as teenager.	-	No	-	-	-
Facial dysmorphism	Coarse facial features, prominent forehead, epicanthic folds, broad nasal bridge	Coarse facial features, low anterior hairline	Coarse facial features	Coarse facial features	No	No (just a right preauricular skin tag)	Coarse facial features	-	1/4
Digital abnormalities	Tapering fingers; short 5th metacarpals; very short 3rd and 4th toes	-	Short 3rd, 4th and 5th metacarpals; wasting of the intrinsic muscles of hands with clawing of the fingers	Short thumbs; marked muscle wasting of the small muscles of hands with clawing of his fingers	-	-	2-4 toe cutaneous syndactyly	-	-
Mirror movements	Yes (fingers)	Yes (fingers)	-	Yes	Yes (hand)	-	-	-	-
Other	Thick dry curly hair, low anterior hairline, iron deficiency anaemia, muscular ventricular septal defect, mongolian blue spot, long sighted	Thick dry curly hair, squint, iron deficiency, anaemia	Bicuspid aortic valve	Hypothyroidism	-	-	-	Hyperpigmentation of the skin in the form of small café au lait macules	3 with ataxia (1 too young for assessment); 1 with early closure of sutures; 2 with malformed chest (1 abnormal-shaped and enlarged chest and 1 mild pectus excavatum)